

The Requirements of a Nuclear Propulsion System for the Human Exploration of Mars

A Thesis Presented

by

Scotia R. Rollins

To the Department of Natural Sciences

of

Scripps and Pitzer Colleges

In Partial Fulfillment of

The Degree of Bachelor of Arts

Senior Thesis in Physics

April 28, 2025

Contents

List of Figures	iii
List of Tables	vii
1 The Motivation for Nuclear Propulsion	2
1.1 Science on the Surface of Mars	2
1.2 Determining Propulsive Requirements for Mars	4
1.2.1 Calculating ΔV	7
1.2.2 Initial-to-Final Mass Ratio and Specific Impulse Estimations	19
2 Nuclear Propulsion Systems	23
2.1 Introduction	23
2.1.1 The History of Nuclear Propulsion	24
2.2 Nuclear Thermal Propulsion Overview	29
2.2.1 NTP Fuel and Propellant Options	30
2.3 Nuclear Electric Propulsion Overview	31
2.3.1 NEP Fuel and Propellant Options	34
2.3.2 EP Thrusters	35
2.4 Comparison of NEP and NTP	35
3 Trajectory Modeling & Mission Architecture Analysis	38
3.1 Introduction: Trajectory Types	38

3.2	Trajectory Modeling	41
3.2.1	Identifying Launch Windows: Preliminary ΔV and Trajectory Plots .	42
3.2.2	Optimizing Transit Duration and ΔV	46
3.3	Conjunction-Class Mission Analysis	50
3.4	Opposition-Class Mission Analysis	54
3.5	Final Thoughts	58
A	NEP Synergies with Surface Power Generation	59
B	Trajectory Modeling Python Code	61
	Bibliography	64

List of Figures

1.1	A selection of photos taken by NASA's Perseverance Rover showing geologic features of scientific interest [1].	3
1.2	A Hohmann transfer from between Earth and Mars. The first ΔV contribution occurs at the perihelion of the transfer orbit, causing the spacecraft to leave its parking Earth orbit and enter the transfer orbit. The second ΔV contribution occurs at the aphelion of the transfer orbit, causing the spacecraft to be captured by Mars' gravity and leave the transfer orbit.	10
1.3	Schematic of a combined maneuver integrating the second Hohmann transfer burn with an orbital plane change at the ascending node.	17
2.1	Photo of a nuclear thermal engine from the NERVA program.	28
2.2	Nuclear Thermal Propulsion engine. Image courtesy of NASA Glenn Research Center [2].	29
2.3	Nuclear Electric Propulsion system diagram [3].	32
3.1	A comparison of two possible trajectories representative of conjunction- and opposition- class missions. [4].	40

3.2 A plot of total mission ΔV (outbound & inbound) vs. launch date for the following transit durations: 170 days (blue), 180 days (yellow), 190 days (green), 200 days (red), 210 days (purple), 220 days (brown). Launch dates span from January 2037 to October 2041 and occur on the 1st, 10th, and 22nd of each month. The missions shown here have symmetric outbound and inbound trajectories and a Mars surface duration of 40 days.	43
3.3 A plot of outbound ΔV vs. launch date for the following transit durations: 170 days (blue), 180 days (yellow), 190 days (green), 200 days (red), 210 days (purple), 220 days (brown). Launch dates span from January 2037 to October 2041 and occur on the 1st, 10th, and 22nd of each month. Launch opportunities are considered to be the ΔV troughs. This plot shows 3 possible launch windows occurring in 2037, 2039, and 2041. The 2039 launch window is circled and examined in subsequent analysis.	44
3.4 A sample plot of the hyperbolic trajectory corresponding to the first ΔV peak, a local maximum, in 3.3 with a launch date of June 1, 2038 and a Mars arrival date of January 7, 2039 (a 220-day transit). The total ΔV for this 2-burn outbound trajectory is 67.8 km/s, a maximum with respect to other possible launch dates, and highly nonoptimal trajectory choice.	45

3.5 A closer look at the 2039 launch window: Launch date vs. minimum out-bound ΔV for a range of dates in Autumn 2039. The contours represents the change in outbound ΔV over time for different transit durations, as in Figure 3.3. The black data points represent minimum ΔV values for each transit duration, and are fitted with a piecewise polynomial (spline) curve. Although the shorter transit durations may not be technically feasible, they are included in this plot to demonstrate the ΔV magnitudes they require. This plot demonstrates an optimization tradeoff between ΔV , transit duration, and launch date. The circled data points correspond to trajectories shown in Figure 3.7, and are color-coded. The green circle shows the global-minimum ΔV conjunction-class trajectory (250 days) for all trajectories in the launch window, including ones with transit durations greater than 250 days. The orange circle shows an example of an infeasible trajectory with excessive ΔV . The red and blue circles show possible opposition-class trajectories, selected based on the relationship shown in Figure 3.6.

47

3.6 Plot showing the exponential relationship between decreases in transit duration and ΔV . Circled data points correspond to where slope exceeds 0.05 and 0.1, based on suggested ratios to identify opposition-class trajectories. The corresponding transit durations for these data points are 190 days and 150 days.

48

3.7 A comparison of trajectory options corresponding to the circle data-points in Figure 3.5, color matched. The top left image shows the identified conjunction-class option, the global minimum ΔV trajectory within the 2039 launch window with a 250-day outbound transit. The bottom right shows an example of an infeasible trajectory with a very short transit duration (70 days) and very high ΔV (29.13 km/s). The top right and bottom left images show intermediate ΔV opposition-class trajectories (190 and 150 days respectively), identified using slope thresholds in Figure 3.6.	50
3.8 The trajectory plot for the conjunction-class mission chosen for analysis of propulsive requirements, with the minimum calculated ΔV in the 2039 launch window. The outbound ΔV and transit duration are 7.2 km/s and 250 days, the surface duration is 421 days, and the inbound ΔV and transit duration are 6.33 km/s and 295 days. This gives a total mission duration of 966 days and a round-trip ΔV of 13.53 km/s, excluding launch and descent stages. . .	51
3.9 Two opposition-class trajectories: Option 1 is a short-duration, high ΔV (36.81 km/s) mission and Option 2 is a longer-duration, lower- ΔV (21.96 km/s) mission, which uses a long duration (520 days) inbound transit. . . .	55

List of Tables

1.1	Variables, descriptions, calculations, and values for a ΔV calculation of a Hohmann transfer from Earth to Mars (outbound journey)	13
1.2	Summary of the mass breakdown for a possible crewed Mars transfer vehicle using nuclear thermal propulsion outlined in the NASA Human Exploration of Mars Design Reference Architecture 5.0 [4].	20
2.1	Comparison of Estimated Characteristics for NTP and NEP	37
3.1	Mass ratios and I_{sp} requirements for NTP and NEP under two opposition-class mission options. Feasibility ratings (1-4, with 1 being the most feasible) are attributed on the basis of whether these requirements align with allowed ranges (mass ratio ranges are approximated in this section and I_{sp} ranges are outlined in Table 2.1.	56

Abstract

This thesis investigates the propulsion requirements for a crewed mission to Mars, focusing on how mission architecture, particularly the choice between opposition- and conjunction-class trajectories, influences the selection between nuclear thermal propulsion (NTP) and nuclear electric propulsion (NEP). By applying the Tsiolkovsky rocket equation, the Delta-V (ΔV) needed for efficient interplanetary transfers is shown to exceed the performance limits of chemical propulsion, motivating the need for nuclear alternatives.

An engineering comparison of NTP and NEP systems evaluates key parameters including specific impulse, thrust, propellant mass fraction, system mass, and power-to-mass ratios. NTP provides high thrust but moderate efficiency, making it suitable for short-duration missions; NEP offers high efficiency but low thrust, aligning better with long-duration profiles. Trajectory modeling, developed in Python using poliastro and NASA JPL ephemeris data, identifies viable launch windows and quantifies propulsive demands for each mission type.

The analysis demonstrates that NEP may have broader viability across different mission architectures and allow for more conservative mission design. These findings emphasize the importance of aligning propulsion system development with mission architecture early in the planning process. As agencies target a 2039 launch window, strategic investment in the appropriate nuclear propulsion technologies is critical to enabling sustainable human exploration of Mars.

Acknowledgements

I would like to sincerely thank Professor Janet Sheung for her guidance and support throughout the development of this thesis. While challenging my thinking and demanding rigor, she consistently offered constructive advice and insightful feedback that shaped the trajectory of this thesis—Her mentorship has been invaluable. I also express my gratitude to Dean Ulysses Sofia for his thoughtful feedback and support as a second reader.

Chapter 1

The Motivation for Nuclear Propulsion

1.1 Science on the Surface of Mars

In the past century, scientific advancements toward understanding the Solar System and its bodies have been extraordinary. Crewed missions such as Apollo and robotic missions such as Cassini have provided a wealth of imagery, data, and samples that have transformed our knowledge of the Moon and the planets.

Mars exploration initiatives, in particular, have seen dramatic successes through recent robotic missions. The Perseverance and Curiosity rovers continue to return detailed photographs and scientific data, revealing a planet with a complex and dynamic history. With the major discovery of polar ice, evidence for extensive subsurface water reservoirs, and the detection of organic compounds [5], Mars remains one of the most promising candidates in the Solar System for harboring signs of past or present life.

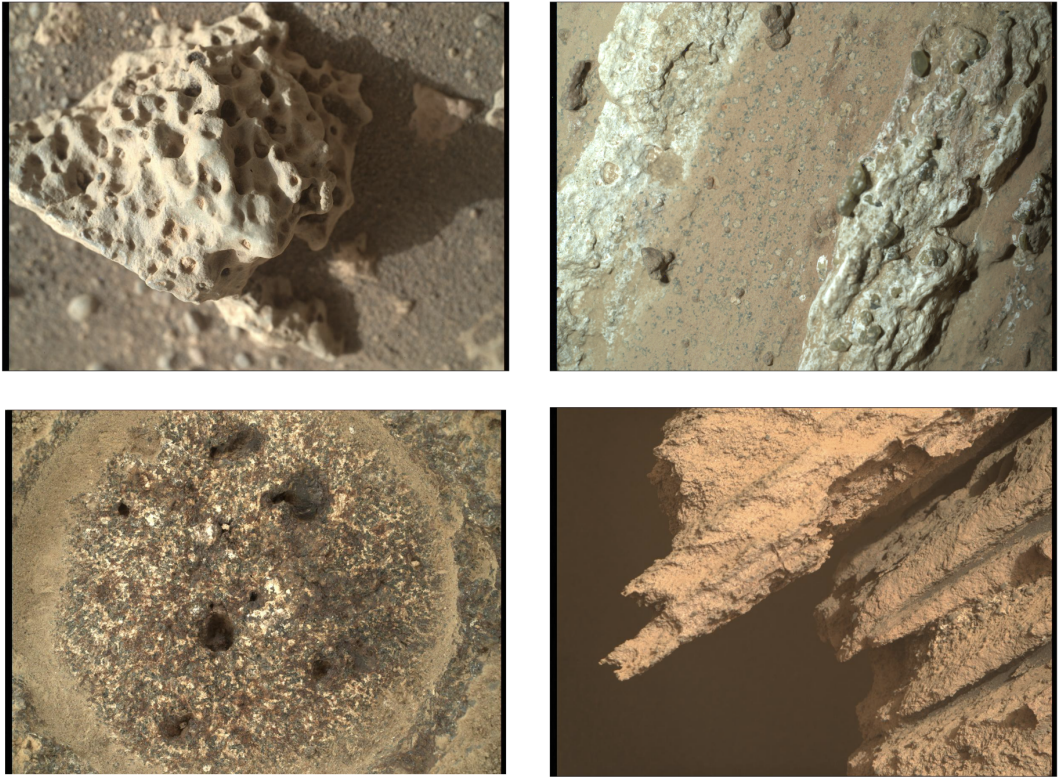


Figure 1.1: A selection of photos taken by NASA’s Perseverance Rover showing geologic features of scientific interest [1].

Despite these achievements, significant scientific limitations inherent to robotic exploration motivate the case for human missions. Among these are constraints on the types and quality of the samples collected, as well as the long delays between sample acquisition and detailed analysis. Crewed missions would enable immediate *in situ* testing and allow for the use of more sophisticated technologies such as deep drilling, which is particularly important given evidence of subsurface water. Such capabilities would dramatically enhance efforts to characterize Mars’ geologic history and assess its past and present habitability. More broadly, they would deepen our understanding of the processes that shaped not only Mars but the Solar System as a whole.

However, the prospect of a crewed Mars mission involves the great challenge of safely transporting a crew to and from Mars, which is associated with the enormous technical challenge of minimizing mission duration by decreasing transit time. These challenges can

only be overcome with advanced propulsion systems capable of the unique constraints of a human mission to Mars, including stringent time, mass, and safety requirements. This necessity is the primary motivation behind efforts in research and development of space nuclear propulsion technologies.

1.2 Determining Propulsive Requirements for Mars

Building an engine that is able to generate enough thrust is one of the greatest technical challenges facing manned space exploration initiatives, made imperative by the necessity of reducing the time in space to minimize the risk of crew health deterioration due to environmental hazards such as radiation. Therefore, it is crucial to know the minimum amount of thrust the propulsion system must be able to produce based on mission architecture constraints, that is, the high-level elements of the mission, such as the duration spent in transit and on the surface of Mars, and the payload mass requirements corresponding to scientific equipment and crew health needs.

Thrust is the resultant force due to the engine's acceleration of gas out of its nozzle, opposite to the direction of travel. The primary factors that contribute to the amount of thrust generated are the amount of fuel burned and the efficiency of the engine in converting that fuel to energy. So, thrust is a ‘pure’ quantity in the sense that on its own, it does not capture the physical aspects of propulsion such as fuel efficiency, just the magnitude of force resulting from that fuel use.

In theory, chemical rockets, which generate thrust through fuel combustion, can produce thrust levels on par with nuclear rockets—it would simply require far larger quantities of fuel to achieve this due to the lesser amount of energy combustion yields compared to nuclear fission. This is because nuclear bonds far exceed chemical bonds in strength, releasing much more energy when they are broken. Beyond this, a major factor that determines the amount of thrust the engine is able to produce is how efficiently it is able to convert that energy into

exhaust velocity (c), since thrust is the product of exhaust velocity and the propellant mass flow rate (1.4).

In evaluating engine types for human Mars exploration, it is necessary to consider the specific impulse (I_{sp}), a measure of engine efficiency that describes the amount of thrust produced per unit mass of fuel expended (1.4). The ability of nuclear propulsion to generate significantly greater I_{sp} is part of what makes it superior to traditional chemical propulsion in the context of deep-space exploration. Nuclear propulsion includes a wide range of technologies, all of which require significant research, development, and testing prior to the baseline mission (the baseline mission refers to the first crewed mission to Mars, which may or may not be proceeded by a further follow-up mission, crewed or uncrewed). Among these technologies are nuclear thermal propulsion (NTP) and nuclear electric propulsion (NEP). Differences in the way fuel is converted to energy and how that energy is used to generate thrust in each of these propulsion types result in significant variation with regard to thrust capabilities—these technical differences are explored in chapter 2.

The purpose of this section is to provide a theoretical background for the mechanisms of thrust generation, particularly with regard to specific impulse (I_{sp}) and ΔV , the change in velocity corresponding to the thrust used over a maneuver, or to each fuel burn. This will contextualize the comparison between NTP and NEP based on these parameters in chapter 2. This chapter will also demonstrate the necessity of nuclear propulsion by calculating the ΔV needed in an efficient trajectory to Mars, and a corresponding I_{sp} value. The guiding equation used in this calculation is the Rocket equation, as expressed in (1.1), which illustrates the relationship between a spacecraft’s initial to final mass ratio ($\frac{M_0}{M_f}$), exhaust velocity (c), and ΔV :

$$\Delta V = c \cdot \ln\left(\frac{M_0}{M_f}\right) \quad (1.1)$$

Each of these variables can be constrained by considering mission architecture and space-craft trajectory requirements. By narrowing in on a value or range of values for both the

payload mass ratio and ΔV , it is possible to determine the necessary I_{sp} using the following relationship, which states that I_{sp} is exhaust velocity (c) divided by acceleration due to gravity (g):

$$I_{sp} = \frac{c}{g} \quad (1.2)$$

Thus, the rocket equation can be expressed as

$$\Delta V = I_{sp} \cdot g \cdot \ln\left(\frac{M_0}{M_f}\right) \quad (1.3)$$

I_{sp} is critical in evaluating different propulsion systems because mathematically, it is the ratio of rocket thrust produced and mass flow rate (\dot{m}) through the engine nozzle [6](1.4). Thrust (F) is simply the force that is equal in magnitude and opposite in direction (by Newton's third law) to the mass expelled by the engine and is directly proportional to the engine's I_{sp} . Thus, I_{sp} is essentially a measure of engine efficiency—the higher it is, the greater the forward force per amount of propellant burned. The unit for I_{sp} is seconds, which can be interpreted as the time for which a unit of propellant can sustain thrust.

$$F = c \cdot \frac{dm}{dt} = I_{sp} \cdot g \cdot \frac{dm}{dt} \quad (1.4)$$

Because the amount of thrust generated depends not only on I_{sp} but also on \dot{m} , the proportionality between I_{sp} and the thrust can vary between different types of propulsion system. For example, nuclear thermal propulsion (NTP) systems typically generate lower I_{sp} than nuclear electric propulsion (NEP) systems but generate comparatively high thrust due to having a higher fuel mass flow rate and differences in how the two systems convert fuel into power to generate thrust (see chapter 2 for more details). Which of these parameters should be prioritized, and thus which type of nuclear propulsion is more advantageous, may depend on mission-specific trajectory requirements, which will be explored in chapter 3.

Today's best chemical rockets produce an I_{sp} of ~ 465 s, while present nuclear thermal

rockets can achieve ~ 900 s, nearly double that of the best chemical rockets, although this may still be far from what is needed for a successful Mars mission. The Institute of Nuclear Energy Safety Technology estimated that a required I_{sp} of 10000s to get to Mars in a month [7], although such a fast journey may not be necessary—mission concepts outlined in NASA’s Human Exploration of Mars Design Reference Architecture 5.0 Document suggest that interplanetary transit time can vary anywhere between 60 and 760 days to minimize ΔV in a short-stay opposition-class mission and between 60 and 360 days for a long-stay conjunction-class mission architecture [8]. Mission architecture options will be explored in chapter 3.

1.2.1 Calculating ΔV

The ΔV needed to accelerate a spacecraft to Mars and back to Earth depends on the type of trajectory taken, which depends on the relative positions of Mars and Earth at the time of launch. To estimate this value, the approach used here begins by calculating ΔV for a highly simplified, maximally efficient trajectory and implementing subsequent corrections to the initial assumptions. Rather than using the rocket equation (1.3) to calculate ΔV , which would require a priori knowledge of the I_{sp} and payload mass ratio, this calculation uses orbital dynamics to arrive at a ΔV value which can then be applied to the rocket equation to identify I_{sp} . An expression for the velocity of an object in orbit can be derived from Kepler’s laws—known as the Vis-Visa equation (1.6)—and will be used to determine the velocity of the spacecraft at different positions of the maneuver from Earth to Mars.

The Hohmann Transfer

Determining the ideal trajectory from Earth to Mars is complicated by the fact that the distance between the two planets changes constantly because of differences in the eccentricity, altitude, and inclination of both planets’ orbits—in other words, their shape, size, and angle. At any given time, the exact distance between them ranges from roughly 55 to 400 million

km¹ with an average distance of 225 million km. In the context of determining the minimum required thrust for such a maneuver, which requires maximizing energy efficiency, the ideal trajectory to take is not a straight line between the two planets when they are at their closest, but an elliptical transfer orbit that intersects both planetary orbits. So, ignoring differences in orbital eccentricity and inclination, the maximally efficient trajectory from Earth to Mars can crudely be understood as a change in altitude of a heliocentric orbit, as the Sun would be the central body of the transfer orbit.

Known as a Hohmann transfer, this type of trajectory requires the minimum amount of propellant because it is only necessary to burn fuel twice to achieve the change in orbital altitude (from Earth orbit to Mars orbit). In this maneuver, the first engine thrust occurs at the point where Earth's Solar orbit intersects with the perihelion of the transfer orbit, which is the closest point of the spacecraft to the Sun in the ellipse, in the tangential direction to Earth's orbit, accelerating the spacecraft into the transfer orbit. The second engine thrust occurs at the intersection of the aphelion of the transfer orbit, which is the farthest point of the spacecraft from the Sun in the transfer orbit, and the final Mars orbit, again tangentially to the direction of orbit. The changes in velocity necessary to redirect the spacecraft to these respective orbits constitute the total ΔV required for the Hohmann transfer.

It is necessary to address the limitations of the Hohmann transfer model in determining a ΔV estimate for the journey from Earth to Mars, which result from several approximations and assumptions made when applying it to this situation. A true Hohmann transfer occurs between two circular orbits, while Earth and Mars follow elliptical heliocentric orbits. This means that, in reality, the departure and arrival velocities vary depending on the positions of the planets within their orbits, making the actual optimal launch windows more constrained than if the orbits were perfectly circular. Additionally, the Hohmann transfer assumes that the initial and final orbits have the same inclination, thus ignoring the ΔV needed to make an orbital plane change. Because Earth and Mars have a non-zero inclination difference

¹NASA Mars Fact Sheet

($\sim 1.85^\circ$), a further correction ΔV must be made; see Section 1.2.1 for this.

Another limitation of the Hohmann transfer model is that it neglects the gravitational influences of Earth and Mars. The sphere of influence (SOI) of a planet is the region within which its gravity dominates over that of the Sun. The Hohmann transfer only describes a change in heliocentric orbit, as if the planets were not there. In reality, a significant ΔV is required to escape Earth’s SOI, which is why most of the propellant consumption occurs during the initial launch from Earth. Similarly, the gravitational effects of Mars play a significant role in the maneuver out of the elliptical transfer orbit, which are not accounted for merely in the change of heliocentric orbital altitude described in this Hohmann transfer.

For these reasons, the best way to understand the ΔV estimate corresponding to an interplanetary Hohmann transfer is as only one part (the greatest part in terms of distance) of the complete trajectory. To refine the ΔV estimate for the full journey, the ‘patched conic’ approach incorporates the Hohmann transfer with maneuvers to escape planetary SOIs and change orbital planes. Nevertheless, the Hohmann transfer model is of great use in determining a maximally efficient trajectory, which is of interest in the context of determining the impulse requirements of a spacecraft engine.

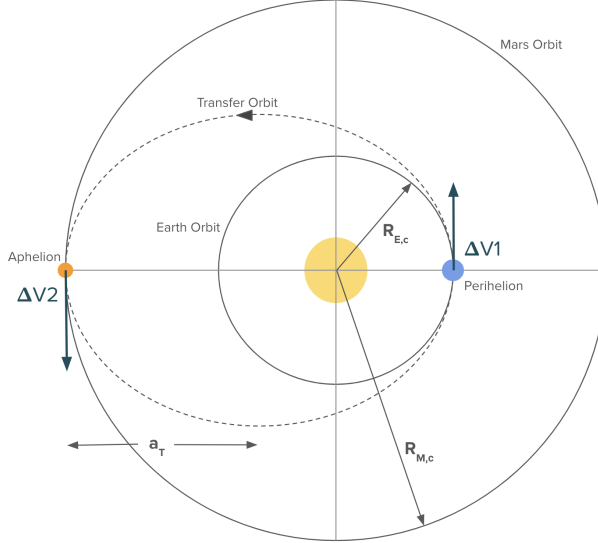


Figure 1.2: A Hohmann transfer from between Earth and Mars. The first ΔV contribution occurs at the perihelion of the transfer orbit, causing the spacecraft to leave its parking Earth orbit and enter the transfer orbit. The second ΔV contribution occurs at the aphelion of the transfer orbit, causing the spacecraft to be captured by Mars' gravity and leave the transfer orbit.

Derivation of the Vis-Visa Equation

Calculating the ΔV expenditure for a Hohmann transfer is straightforward using Leibniz's Vis-Visa equation, which expresses velocity in terms of the relative masses of an object in orbit and the central body and the distance of that object from the central body. A derivation for this equation is presented here, beginning with the expression of velocity in polar coordinates.

$$\begin{aligned}
 v^2 &= v_x^2 + v_y^2 \\
 &= (\dot{r} \cos(\theta) - \dot{\theta} r \sin(\theta))^2 + (\dot{r} \sin(\theta) - \dot{\theta} r \cos(\theta))^2 \\
 &= \dot{r}^2 \cos^2(\theta) - 2\dot{r}\dot{\theta} \sin(\theta)\dot{r} \cos(\theta) + \dot{r}^2 \sin^2(\theta) + \dot{r}^2 \sin^2(\theta) + 2\dot{r}\dot{\theta} \sin(\theta)\dot{r} \cos(\theta) + \dot{r}^2 \dot{\theta}^2 \cos^2(\theta) \\
 &= (\dot{r}^2 + r^2 \dot{\theta}^2) \cdot (\sin^2(\theta) + \cos^2(\theta)) \\
 &= \dot{r}^2 + r^2 \dot{\theta}^2
 \end{aligned}$$

This states that an object's velocity squared is the sum of its radial velocity squared and the product of its angular velocity squared and its radial distance squared. We now need to express r in terms of known distances, such as the semi-major axis (a_T). Kepler's first law tells us that, for an elliptical orbit, the radial distance of an object from the central body is:

$$r = \frac{a_T(1 - e^2)}{1 + e \cdot \cos(\theta)} \quad (1.5)$$

Note that a_T represents the semi-major axis of the transfer orbit and is defined as the distance between the center of the ellipse and its largest radius. For the above Hohmann transfer, this is: $a_T = \frac{R_{E,c} + R_{M,c}}{2}$. e represents the eccentricity of the elliptical orbit, which is a measure of its deviation from a circular orbit, i.e., how elliptical it is—it can be calculated as $e = \frac{R_{M,c} - R_{E,c}}{R_{M,c} + R_{E,c}}$, however, this is not necessary in the calculation of ΔV using the Vis-Visa equation.

We can take the derivatives of r and θ and plug them into the above expression for velocity²:

$$\begin{aligned}\dot{r} &= \frac{a_T(1 - e^2) \sin(\theta) \cdot \dot{\theta}}{(1 + e \cdot \cos(\theta))^2} \\ &= \frac{r^2}{a_T(1 - e^2)} \cdot e \cdot \sin(\theta) \cdot \dot{\theta} \\ \dot{\theta} &= \frac{h}{r^2} \\ h &= \sqrt{\mu a_T(1 - e^2)} \\ \dot{\theta} &= \frac{\sqrt{\mu a_T(1 - e^2)}}{r^2} \\ \dot{r} &= \sin(\theta) \cdot e \cdot \sqrt{\frac{\mu}{a_T(1 - e^2)}}\end{aligned}$$

Above, h is the specific angular momentum of the object, i.e., its angular momentum per unit mass, and μ is the standard gravitational parameter of the central body, $\mu = G(M+m)$. Performing some algebra here, we obtain the Vis-Visa equation, which expresses an object

²See FIU Orbital Mechanics PDF for more details on this derivation.

in orbit's velocity in terms of its radial distance r from the central object:

$$v = \sqrt{\mu \left(\frac{2}{r} - \frac{1}{a_T} \right)} \quad (1.6)$$

Using this equation, a value for ΔV is easily obtained by finding the difference between the velocities of the object in the initial and final orbits. Table 1.1 displays the relative values to perform this calculation.

Applying the Vis-Visa Equation

Having derived the Vis-Visa equation, it is now possible to calculate the total ΔV for a Hohmann transfer from Earth to Mars by determining four velocities at different stages of the trajectory. The first is the orbital velocity of the spacecraft at Earth's orbital altitude. The second velocity is the initial velocity of the spacecraft in the transfer orbit—the difference between these two velocities is the change in velocity needed to redirect the spacecraft into the transfer orbit, and the first of the two ΔV contributions of the Hohmann transfer. The third velocity is the final velocity of the spacecraft in the transfer orbit, where it is ready to accelerate into its final orbit, which is the velocity with which it orbits the sun at the orbital altitude of Mars. Again, the difference between the third and fourth velocities constitutes the second ΔV contribution of the Hohmann transfer. Table 1.1 shows the relevant variables and calculations.

Variable	Description	Calculation	Value & Units
$R_{E,c}$	radius of initial orbit, i.e., Earth solar orbit, approximated as circular	avg. of Earth perihe- lion and Earth aphelion ³	$1.496 \cdot 10^8$ km
$R_{M,c}$	radius of final orbit, i.e., Mars' solar orbit, approximated as circular	avg. of Mars perihe- lion and Mars aphelion ⁴	$2.28 \cdot 10^8$ km
a_T	semi-major axis of the transfer orbit (out- bound and inbound journeys)	$a_T = \frac{R_{E,c} + R_{M,c}}{2}$	$1.89 \cdot 10^8$ km
μ	standard gravitational parameter of the cen- tral body, the Sun	$\mu = G \cdot (M + m) \approx$ $G \cdot M_{\odot}$	$1.327 \cdot 10^{11}$ $\text{km}^3 \cdot \text{s}^{-2}$
$v_{E,c}$	initial velocity in Earth orbit (out- bound journey)	$v_{E,c} = \sqrt{\frac{\mu}{R_{E,c}}}$	$29.783 \text{ km} \cdot \text{s}^{-1}$
$v_{T,i}$	velocity at transfer or- bit intercept 1 (Earth)	$v_{T,i} = \sqrt{\mu \left(\frac{2}{R_{E,c}} - \frac{1}{a_T} \right)}$	$32.728 \text{ km} \cdot \text{s}^{-1}$
$v_{T,f}$	velocity at transfer or- bit intercept 2 (Mars)	$v_{T,f} = \sqrt{\mu \left(\frac{2}{R_{M,c}} - \frac{1}{a_T} \right)}$	$21.478 \text{ km} \cdot \text{s}^{-1}$
$v_{M,c}$	velocity at transfer or- bit intercept (Mars)	$v_{M,c} = \sqrt{\frac{\mu}{R_{M,c}}}$	$24.127 \text{ km} \cdot \text{s}^{-1}$

Table 1.1: Variables, descriptions, calculations, and values for a ΔV calculation of a Hohmann transfer from Earth to Mars (outbound journey).

Now, all that is required is some simple addition:

$$\begin{aligned}
\Delta V1 &= v_{T,i} - v_{E,c} \\
&= 32.728 \text{ km/s} - 29.783 \text{ km/s} \\
&= 2.945 \text{ km/s} \\
\Delta V2 &= v_{M,c} - v_{T,f} \\
&= 24.127 \text{ km/s} - 21.478 \text{ km/s} \\
&= 2.649 \text{ km/s} \\
\Delta V_{tot} &= \Delta V1 + \Delta V2 \\
&= 5.594 \text{ km/s}
\end{aligned}$$

The total ΔV required to make a Hohmann transfer from Earth to Mars is approximately 5.6 km/s. Although this type of trajectory is highly ideal and relies on numerous simplifying approximations, it is valuable in that it demonstrates the order of magnitude of ΔV for an efficient interplanetary transfer outside of launch and descent ΔV requirements. The ΔV required to launch a spacecraft into a low Earth orbit (LEO) usually falls within 9.3-10 km/s [9]. This Hohmann transfer calculation therefore shows that the majority of the propellant usage may not necessarily go towards the interplanetary transfer, but may occur in the launch stage.

Transfer Time and Alternative Trajectories

The time that the Hohmann transfer maneuver would take is easily calculated using Kepler's 3rd law, which observes a proportional relationship between an orbit's period (P) and semi-major axis (a):

$$P^2 = \left[\frac{4 \cdot \pi^2}{G \cdot (m_1 + m_2)} \right] \cdot a^3 \quad (1.7)$$

Here, $G \cdot (m_1 + m_2)$ in the denominator is the standard gravitational parameter (μ) from before. Again, because the mass of the spacecraft is negligible compared to the central body of the orbit (the Sun), this expression can be rewritten as $G \cdot M_{\odot}$. A Hohmann transfer occurs over exactly half of an elliptical orbit, so the time taken for it is half of the orbital period and can be calculated as follows.

$$\begin{aligned} t_{Hoh} &= \frac{1}{2} \cdot P \\ &= \frac{1}{2} \cdot \sqrt{\frac{4 \cdot \pi^2 \cdot a^3}{G \cdot M_{\odot}}} \\ &= 2.237 \cdot 10^7 \text{ s} \\ &= 259 \text{ days} \end{aligned}$$

The time corresponding to this maximally energy-efficient Hohmann transfer is approximately 259 days. Reducing the transfer time requires moving beyond the Hohmann transfer and using a higher energy trajectory. This can be done by increasing the departure ΔV , which causes the transfer orbit to become more elliptical, and would require greater ΔV upon arrival at Mars. If the departure ΔV is sufficiently increased, eventually the trajectory is no longer elliptical but hyperbolic—generally, the greater the departure ΔV , the more the trajectory resembles a straight line.

In addition to decreasing transfer time, an appeal of using a higher departure velocity is the possibility of aerocapture, in which the planet's atmospheric drag is used to slow down the spacecraft, rather than impulse. This technique is of great economic appeal in such high-cost missions, in terms of propellant, though the requirement for greater departure impulse may counteract such a benefit. Although aerocapture has been used on robotic missions to

Mars, as in NASA’s Viking Program in the 1970s⁵, it is a feat that becomes increasingly difficult with higher payload masses, as would be the case in a crewed mission, due to the greater drag that would be needed to decelerate the spacecraft. This high payload mass would also require a much higher departure impulse than in a robotic mission to achieve a hyperbolic trajectory. So, in the context of human Mars exploration, an elliptical transfer orbit is probably more feasible than a hyperbolic one.

Patched-Conic ΔV Approximation

This section builds upon the ΔV estimate for a basic Hohmann transfer by incorporating the ΔV contributions from the other trajectory sections, including planetary ascent and descent stages and the inbound transfer maneuver, in a patched-conic approach. First, the Hohmann transfer ΔV estimate must be corrected to account for the orbital plane difference between the planets.

To maneuver from the orbital plane of Earth to that of Mars, an additional velocity change is required beyond the altitude change described by the Hohmann transfer. Although orbital plane changes can be costly in ΔV , the inclination difference (Δi) between Earth and Mars is relatively modest at 1.85° , especially compared to Earth-Moon (5.1°) and Earth-Mercury (7.0°) inclination differences [10]. We consider two approaches for executing a plane change: a simple plane change involves a separate burn to the transfer orbit, while a combined plane change is performed simultaneously with one of the transfer burns.

A simple plane change involves a third impulse at the ascending node, where the Earth and Mars orbital planes intersect. Since this maneuver alters only the direction (not the magnitude) of the velocity vector, the initial and final velocities form an isosceles triangle. By trigonometry:

⁵NASA Viking Program

$$\begin{aligned}
|\Delta V_{simple}| &= 2 \cdot \sin\left(\frac{\Delta i}{2}\right) \cdot V_{t,f} \\
&= 2 \cdot \sin\left(\frac{1.85}{2} \cdot \frac{\pi}{180}\right) \cdot 24.13 \text{ km/s} \\
&= 0.779 \text{ km/s}
\end{aligned}$$

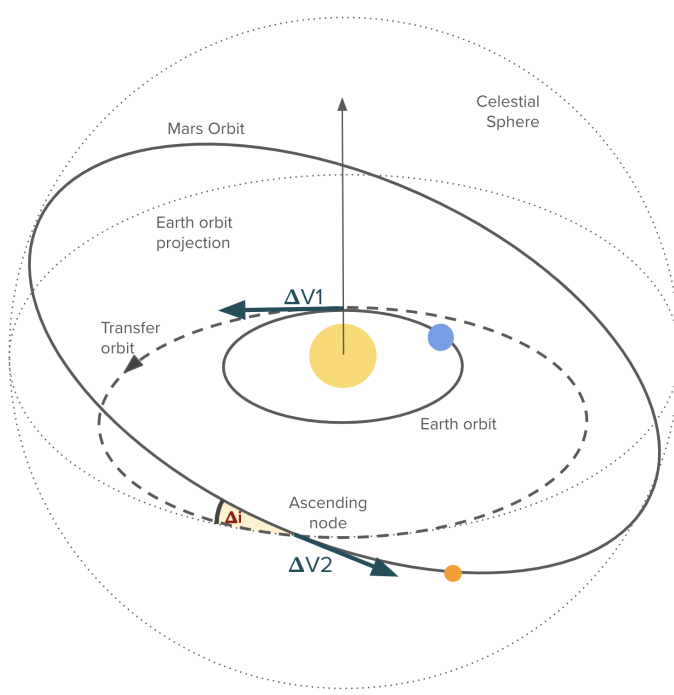


Figure 1.3: Schematic of a combined maneuver integrating the second Hohmann transfer burn with an orbital plane change at the ascending node.

A more efficient strategy is to combine the plane change with the second Hohmann burn, as illustrated in Figure 2.2. In this case, the initial and final vectors differ in both direction and magnitude, forming a scalene triangle. Applying the law of cosines:

$$\begin{aligned}
\Delta V_{combined}^2 &= V_{t,f}^2 + V_{M,c}^2 - 2 \cdot V_{t,f} \cdot V_{M,c} \cdot \cos(\Delta i) \\
&= 24.13^2 + 21.48^2 - 2 \cdot 24.13 \cdot 21.48 \cdot \cos(1.85 \cdot \frac{\pi}{180}) \\
&= 2.75 \text{ km/s}
\end{aligned}$$

Adding this to the first Hohmann burn results in a reduced ΔV of:

$$\Delta V_{total, combined} = 2.94 \text{ km/s} + 2.75 \text{ km/s} = 5.69 \text{ km/s} \quad (1.8)$$

This approach improves ΔV efficiency by approximately 11.3% compared to the simple plane change.

Total Outbound & Inbound ΔV

NASA estimates a ΔV of 25,000 ft/sec ($\sim 7.6 \text{ km/s}$) to launch a spacecraft into a 200-mile high orbit [11]. For Mars descent, Palaszewski estimates a ΔV of 0.812 km/s [12]. Incorporating these values with the Hohmann transfer and combined plane change, the total outbound ΔV is:

$$\Delta V_{outbound} = 7.6 \text{ km/s} + 5.69 \text{ km/s} + 0.812 \text{ km/s} = 14.1 \text{ km/s} \quad (1.9)$$

Assuming a symmetric return trajectory (i.e., a Mars-to-Earth Hohmann transfer), we can expect the inbound transfer ΔV to be approximately the same as the outbound. However, due to differences in the gravitational strengths of Earth and Mars, the ascent and descent ΔV s differ. Palaszewski provides estimates of 4.2 km/s for Mars ascent [13], which is significantly lower than the 7.6 km/s for Earth ascent. For Earth descent, atmospheric drag can be leveraged in an aerobraking technique to reduce propulsive needs, requiring only a small retrograde burn of approximately 0.1 km/s. Therefore, the inbound ΔV is estimated

as:

$$\text{Mars ascent : } 4.2 \text{ km/s}$$

$$\text{Hohmann return + combined plane change : } 5.69 \text{ km/s}$$

$$\text{Earth descent (aerobraking + retrograde burn) : } 0.1 \text{ km/s}$$

$$\Delta V_{\text{inbound}} = 4.2 \text{ km/s} + 5.69 \text{ km/s} + 0.1 \text{ km/s} = 9.99 \text{ km/s} \quad (1.10)$$

Hence, the total round-trip ΔV is approximately:

$$\Delta V_{\text{total}} = 14.10 \text{ km/s} + 9.99 \text{ km/s} = 24.09 \text{ km/s} \quad (1.11)$$

1.2.2 Initial-to-Final Mass Ratio and Specific Impulse Estimations

This section aims to estimate an initial-to-final mass ratio ($\frac{M_0}{M_f}$) in order to identify a I_{sp} requirement using the rocket equation (1.3). The total initial mass of the spacecraft (M_i) can be described in terms of three constituent parts:

$$M_i = M_p + M_s + M_{pay} \quad (1.12)$$

The structural mass (M_s) describes the core infrastructure of the spacecraft, including its structural frame, propulsion system, and power generation system. The crew habitat vehicle likely to be used in the first manned Mars mission is the Orion Multi-Purpose Crew Vehicle (Orion MPCV) produced by Lockheed Martin, which is currently being used in NASA's Artemis program. This vehicle is currently used in tandem with NASA's Space Launch System (SLS) and Exploration Ground Systems (EGS) [14][15].

The payload mass (M_{pay}), describes the components that contribute to the achievement

of mission objectives, including scientific equipment, life support systems (crew habitat, food and water, surface power generation systems, waste management and water recycling systems) and the crew themselves. Different mission architectures, discussed in Chapter 3, lead to significant payload mass differences, but generally the longer the mission, the more payload is required. Different vehicles allow different payload mass fractions ($\frac{M_{pay}}{M_i}$), with vehicles for crewed missions ranging from 0.012 to 0.0538 [16]. However, this range is based on crewed missions that have used chemical propulsion. Because nuclear fission generates more energy than chemical combustion, less propellant is required in nuclear propulsion, potentially allowing for greater payload mass fractions.

The propellant mass (M_p) depends largely on the type of propellant used (discussed in Sections 2.3.1 and 2.2.1—the likely choices are LH₂-LOX for NTP and Argon or Xenon for NEP). Like structural mass, propellant mass depends crucially on elements of the mission architecture such as transit duration and launch timing. A crucial difference between NTP and NEP is their strikingly different requirements for their propellant mass fractions (see Table 2.1), largely due to differences in fuel efficiency (determined by I_{sp}) and thrust generation.

Component	Mass (tons)
Payload (crew, habitat, supplies)	62.8
Structure (tanks, engines, systems)	86
Propellant	207.6
Total Initial Mass	356.4

Table 1.2: Summary of the mass breakdown for a possible crewed Mars transfer vehicle using nuclear thermal propulsion outlined in the NASA Human Exploration of Mars Design Reference Architecture 5.0 [4].

NASA’s Human Exploration of Mars Design Reference Architecture 5.0 (DRA 5.0) provides an estimated mass breakdown (summarized in Table 1.2) for a crewed Mars mission using a nuclear thermal rocket, supported by a separate cargo launch. Based on this DRA 5.0 mass breakdown, the initial-to-final mass ratio ($\frac{M_0}{M_f}$) is 2.395. This indicates that the vehicle’s initial mass, fully fueled, is more than twice its final mass after propellant expen-

diture, meaning that a large proportion of the total initial mass is propellant. If interpreted as a single-launch strategy (i.e., ignoring the separate cargo launch), the initial-to-final mass fraction derived from this breakdown may be an underestimate, resulting in a conservative overestimate of I_{sp} due to their inverse relationship.

Applying this mass ratio (2.395) to the rocket equation (1.3) with a total mission ΔV of 24.09 km/s calculated in Section 1.2.1:

$$24,090 \text{ m/s} = I_{sp} \cdot 9.81 \text{ m/s}^2 \cdot \ln(2.395) \quad (1.13)$$

$$I_{sp} = 2811 \text{ s} \quad (1.14)$$

These estimates yield a specific impulse of 2811 s, corresponding to the I_{sp} capabilities of nuclear electric propulsion technologies (see Table 2.1). However, this should be regarded as a rough estimate due to several simplifying assumptions. The rocket equation assumes an idealized, single-stage system operating in a vacuum, with constant exhaust velocity and no gravitational or drag losses beyond what is already captured in the ΔV . In reality, a crewed Mars mission would involve multi-stage vehicles, variations in thrust efficiency, and complex mission phases (such as orbital insertion, transfer burns, and descent/ascent maneuvers) that are not fully captured by this calculation.

Nevertheless, this estimate provides a useful first-order approximation. Given the known relationships between ΔV , mass ratio, and propulsion efficiency, and drawing on the mass estimates provided by NASA [4], we can expect that the propulsion system for a crewed mission to Mars would require a specific impulse on the order of at least 1000 s to remain within realistic engineering constraints.

While this estimate does not definitively indicate whether nuclear electric propulsion (with specific impulses exceeding 2000 s) or nuclear thermal propulsion (around 900 s) is more suitable for the baseline Mars mission or future deep-space missions, it does make

one thing clear: chemical propulsion systems lack the specific impulse necessary for such endeavors. Consequently, if NASA or the United States is to pursue the human exploration of Mars seriously, the development of nuclear propulsion technologies must be treated as a technological priority and approached strategically.

Chapter 2

Nuclear Propulsion Systems

2.1 Introduction

Nuclear fission occurs when a neutron collides with an atom, causing it to split into smaller atoms and more neutrons, causing a chain reaction that releases vast amounts of energy. For Uranium 235 (U-235), a single atom splitting through fission generates 200 MeV of energy. In chemical combustion, the energy release mechanism for traditional chemical rockets, the burning of a single atom of carbon generates 6 eV. Comparatively, fission releases energy that is over seven orders of magnitude greater than chemical combustion for the same number of atoms. This immense energy density is what makes nuclear energy viable for space propulsion, among many other applications, such as supplying energy to large-scale power grids.

The objective of this chapter is to provide a holistic overview of nuclear propulsion systems, from the history of their development to current efforts and obstacles towards it. The two primary categories of nuclear propulsion technologies are nuclear thermal propulsion (NTP) and nuclear electric propulsion (NEP), both of which use nuclear fission (as opposed to fusion) to generate large amounts of energy. Given the significantly greater energy per fuel mass that is achievable with nuclear propulsion compared to traditional chemical propulsion

systems, they are favorable in the context of deep-space exploration and particularly a crewed Mars mission.

The dilemma surrounding the development of nuclear propulsion technologies is both theoretical and practical. On the one hand, there is ongoing debate over whether NTP or NEP is better suited for a crewed Mars mission given differences in energy efficiency, thrust-to-weight ratios, and other characteristics which have important implications for specific mission constraints such as transit time, payload mass, and onboard power requirements.

On the other hand, both NEP and NTP require careful strategic planning to reach technological maturity, particularly with respect to the allocation of funding and resources, due to the extensive research, development and testing required for each technology [17]¹. Because there is limited overlap in their development pathways, and in the interest of progressing towards human Mars exploration goals, the decision between these technologies is both critical and time sensitive.

As an alternative to fission-based propulsion, concepts exist for nuclear fusion-based propulsion systems. While fusion offers many theoretical advantages to fission, it is not yet viable to the same extent as fission, and these system concepts are far less developed. Appendix ?? offers a brief discussion of fusion-based propulsion technologies, along with current promising efforts in NTP and NEP at NASA.

2.1.1 The History of Nuclear Propulsion

Although nuclear propulsion technology development is at an early stage, particularly in the application to space exploration, initiatives in the research and development of nuclear powered aircraft began nearly a century ago in the United States. In 1946, the U.S. initiated its Nuclear Propulsion Program with the objective of determining the feasibility of nuclear

¹The recommendation of the National Academies of Sciences, Engineering, and Medicine 2021 study on space nuclear propulsion technologies states: “if NASA plans to apply NEP technology to a 2039 launch of the baseline mission, NASA should immediately accelerate NEP technology development.” They also found that, even with an aggressive program, the development of an NTP system capable of executing the baseline mission in 2039 is uncertain, although possible. (p.72)[17].

energy for the propulsion of aircraft, which ran until 1961 [18]. This program, primarily motivated by the increasing demands of the Cold War, developed and tested two types of nuclear thermal propulsion: direct air cycle and indirect air cycle-propulsion models which are still relevant today. The difference between these models is the heat transfer method used in each; in direct air cycle, propellant flows directly through the reactor, rather than using heat exchange between the reactor core and propellant. This leads to greater specific impulse and thrust capabilities, but greater concern of radioactive exhaust risks—it is nevertheless the model used in most modern NTP systems for its propulsive advantage, including the Demonstration Rocket for Agile Cislunar Operations (DRACO) program, one of NASA's most prominent and well-funded NTP programs, in collaboration with the Defense Advanced Research Projects Agency (DARPA), a government defense agency [19].

Efforts in space nuclear propulsion for both military and civilian applications began with Project Rover in 1955 at Los Alamos National Laboratory, which had the specific aim of developing a nuclear thermal rocket for crewed and long-duration space missions [20]. Though it started as a U.S. Air Force project, it was transferred to NASA during the agency's inception in 1958, catalyzed by the Sputnik crisis, in which public anxiety and the geopolitical tension between the U.S. and the Soviet Union during the Cold War was heightened due to the latter's technical achievement with the launches of Sputnik I and II [21], an event often considered to be the birth of the U.S.-U.S.S.R. Space Race. That the history of nuclear propulsion is so deeply associated with the inception of NASA speaks to a long-standing understanding of the potential of nuclear power to transform space exploration capabilities. Likewise, the non-linearity of its development through history reflects the great challenges of contingency on military and political agendas and the corresponding attention and influence from the public domain, evidenced by the ongoing presence of the antinuclear movement².

²The antinuclear movement refers broadly to social opposition to the development of nuclear weapons and energy from nuclear power plants. Motivations for the movement range from environmental and radioactive-waste concerns to moral concerns about the use of nuclear weapons in wars. The movement has seen several periods of significant presence following tragedies at Hiroshima, Chernobyl, and Three Mile Island [22].

A natural question, given this history of nuclear propulsion technologies, is how much ongoing overlap there is between space exploration and military incentives in their continued development. The DRACO program, which saw a funding increase from 37 million USD in FY2022 to 81.98 million USD in FY2024, evidences a significant degree of overlap [23] (Appendix ?? explores the progress of the DRACO program in developing NTP for space applications). Whether or not this military-shared incentive is something to be leveraged to achieve science and space exploration goals, or whether dependence upon external military agencies leads to too much funding uncertainty, risk of project cancelation, or divergence from space-exploration specific requirements, is nuanced. Furthermore, the extent to which ethical and national security concerns should be factored into nuclear propulsion development efforts is beyond the scope of this thesis—but these are important and interesting questions with significant implications.

The most prominent achievements of Project Rover were seen in the Nuclear Engine for Rocket Vehicle Application (NERVA) program, which ran from 1961 to 1973. With the aim of developing a flyable engine as a "Proof of Concept", this program was highly successful and developed testing facilities and eight different nuclear reactors and performed actual launch tests with engines powered by them [20][24]. The results of this program were highly significant because they demonstrated the technical feasibility of a nuclear thermal rocket in producing power levels, temperatures, pressures, and durations that meet modern expectations for an NTP system. A 1991 report by Robbins and Finger stated, regarding the Nuclear Reactor Experimental (NRX), NERVA's main reactor that "The NRX Series demonstrated improved structural integrity, reduced fuel corrosion rates (longer life) and higher temperature operation, in excess of 2200°K. NRX-A6, the last in a series, operated one hour continually. The fuel corrosion rate was low. The extrapolated reactor lifetime, 2-3 hours, would be commensurate with today's manned Mars mission requirement" [24]³.

The extensive research and testing of NTP performed during the NERVA program may

³The maximum power produced by one of the NERVA reactors was 4 GW, which produces approximately 100 tons of thrust.

give NTP an advantage over NEP in terms of its level of technological readiness. The National Academies note that “legacy fuels, materials, and structural design approaches (e.g., from the Rover/NERVA program) could be used to mitigate some schedule and technical risk associated with an NTP system fueled with HEU, if the technology can be fully recaptured and sufficient data are available to identify failure modes and benchmark modern M&S codes used to design the NTP system” [17]. However, given the significant time that has passed since the NERVA program, it remains uncertain whether the necessary technology can be recovered and whether sufficient data still exist.

Nuclear electric propulsion is younger than nuclear thermal propulsion, although it has arguably been more associated with ambitious space exploration initiatives. One of the earliest major applications of NEP concepts was NASA’s Prometheus Project in the early 2000s, which aimed to develop a nuclear-powered spacecraft for missions to the outer planets. The centerpiece of this effort was the Jupiter Icy Moons Orbiter (JIMO), intended to explore Europa, Ganymede, and Callisto. However, the project was canceled in 2005 due to increasing costs and technical challenges [25].

Although NEP studies date back to the 1950s and 1960s under programs such as SNAP (Systems for Nuclear Auxiliary Power) and BES-5 (Buk Electrostatic Spacecraft), which explored small nuclear reactors for space applications [26], no NEP system has yet flown operationally. However, interest in the technology has continued—in recent years, NASA has renewed research efforts into NEP through initiatives like the Power and Propulsion Element (PPE) for the Lunar Gateway, which investigates the integration of high-efficiency electric propulsion with space nuclear power systems [27]. While these efforts reflect a growing recognition of the potential of NEP to enable sustainable crewed missions beyond low Earth orbit, particularly a Mars mission, NEP’s relative lack of technological maturity with respect to NTP may pose a strategic disadvantage with regard to its development prior to the baseline mission.



Figure 2.1: Photo of a nuclear thermal engine from the NERVA program.

2.2 Nuclear Thermal Propulsion Overview

Conceptually, NTP systems operate similarly to traditional chemical propulsion, as both expel heated propellant to generate thrust. The key difference is in the way heat is generated, which is nuclear fission instead of combustion. NTP systems typically use a liquid hydrogen (LH₂), the coldest and lightest known fuel, or other low-molecular-weight fuels, since these provide a higher specific impulse [2]. This is due to an inversely proportional relationship between the molar mass of fuel and the exhaust velocity, as explained by Sutton and Biblarz [9].

A nuclear thermal propulsion system can be broken down into three main subsystems: a nuclear reactor, a rocket engine, and a propellant management and storage system. LH₂ is stored in a cryogenic tank and delivered to the nuclear reactor through turbopumps and propellant management components. In the nuclear reactor, the heat generated by nuclear fission is used to burn LH₂, forming gas that is accelerated out of the nozzle to create thrust. This gives a proportional relationship between an NTP system's thrust (F_{NTP}) and specific impulse (I_{sp}):

$$F_{NTP} = v_{ex} \cdot \dot{m} = I_{sp} \cdot g_0 \cdot \dot{m} \quad (2.1)$$

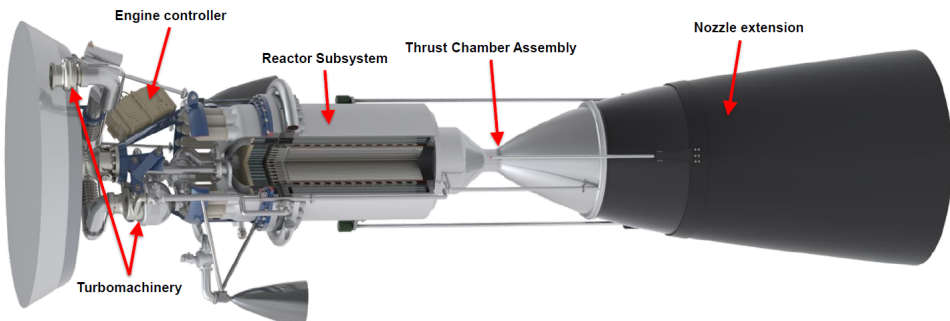


Figure 2.2: Nuclear Thermal Propulsion engine. Image courtesy of NASA Glenn Research Center [2].

In NTP systems, specific impulse capabilities are contingent on the maximum temperatures provided by the nuclear reactor. The $\sim 900\text{s}$ upper limit for I_{sp} outlined in table 2.1 is given with reactor core temperatueres of 2500-2700 K, achieved in the NERVA program [24]. Since the I_{sp} estimate for NTP is based on the performance of systems more than 50 years ago, it is plausible that modern reactor designs may exceed these temperature limits and provide even greater I_{sp} values. An NTP reactor concept developed by the Commonwealth of Independent States (CIS) in the early 1990s has expected temperatures of 3200K, theoretically enabling I_{sp} values that exceed 1000 s [28].

2.2.1 NTP Fuel and Propellant Options

In order to reach Mars, a spacecraft will unavoidably need to burn very large amounts of propellant, which can easily make the spacecraft's initial mass very large. For this reason, choosing a propellant that maximizes energy per mass is crucial. A propellant is simply the combination of a fuel such as LH₂ and an oxidizer such as liquid oxygen (LOX), the most likely combination for an NTP system. It has been used successfully in numerous space launch vehicles, including the US Space Shuttle, the first reusable spacecraft [9]. From an environmental perspective, the LH₂-LOX propellant is ideal because its only chemical output when burned is water. Other common fuels, such as kerosene, produce CO₂ and particulate matter. Hydrogen's low density means that it must be stored at cryogenic temperatures to be stored in liquid form (-423 °F). The same challenge exists with oxygen, which must be stored at -297 °F to be liquid. LH₂ also requires a larger fuel tank because of its low density, which contributes both to greater spacecraft mass and drag—nevertheless, the LH₂-LOX propellant is an optimal choice due to its high specific impulse (due to the molecular weight of hydrogen).

In addition to the main propellant, an NTP system also utilizes a nuclear fuel in the fission process to generate heat. Modern nuclear propulsion systems including NTP and NEP are likely to use a high-assay low-enriched uranium (HALEU) fuel or highly enriched

uranium (HEU), which is composed of more and less 20% uranium-235, respectively. The NERVA program used uranium carbide (UC_2), an HEU fuel. Nuclear fuels are a distinct component of nuclear propulsion that requires both technical and conceptual development and faces unique maturation challenges. The 2021 National Academies study on space nuclear propulsion recommended the comparative assessment of HEU and HALEU on the basis of technical feasibility, performance in NTP vs NEP, safety and security, fuel availability, cost, schedule, and supply chain [17].

2.3 Nuclear Electric Propulsion Overview

Like in nuclear thermal propulsion (NTP), nuclear electric propulsion (NEP) systems generate heat in a nuclear fission reactor. Rather than directly heating the propellant, this heat is converted into electrical power—a similar process used in nuclear power plants. Subsequently, this electrical power is used to accelerate an ionized propellant in electrical thrusters, generating thrust [17].

Although electric propulsion is already in use for uncrewed space missions such as the Psyche mission [29], the thrusters used in these only operate at kilowatt-scale power levels and therefore do not provide enough electrical power to be used in a crewed Mars mission (1.8 -3.6 megawatts is estimated for a short-duration mission [17]). Existing electrical propulsion thrusters are typically powered by solar power. In order to achieve megawatt-scale electrical power, NEP systems would incorporate the enormous energy density provided by nuclear fission.

The reliance of NEP systems on conversion to electrical power has a critical implication for understanding their thrust generation. Specifically, because of the conversion to electrical power rather than direct exhaust of gas, thrust is dependent on the efficiency of the power conversion system.

By definition, the thrust efficiency, η , is given by [26]:

$$\eta = \frac{\dot{m} \cdot v_{ex}^2}{2 \cdot P} \quad (2.2)$$

where \dot{m} is the mass flow rate, v_{ex} is the exhaust velocity, and P is the available electrical power. Since thrust is the product of mass flow rate and exhaust velocity, and considering the energy conversion involved, the thrust generated by an NEP system can be expressed as:

$$F_{NEP} = \frac{2 \cdot \eta \cdot P}{v_{ex}} = \frac{2 \cdot \eta \cdot P}{g_0 \cdot I_{sp}} \quad (2.3)$$

where g_0 is the standard gravitational acceleration and I_{sp} is the specific impulse. Here, there is an inverse relationship between thrust and specific impulse, unlike in NTP. This explains why NEP systems achieve high specific impulse values but produce low thrust.

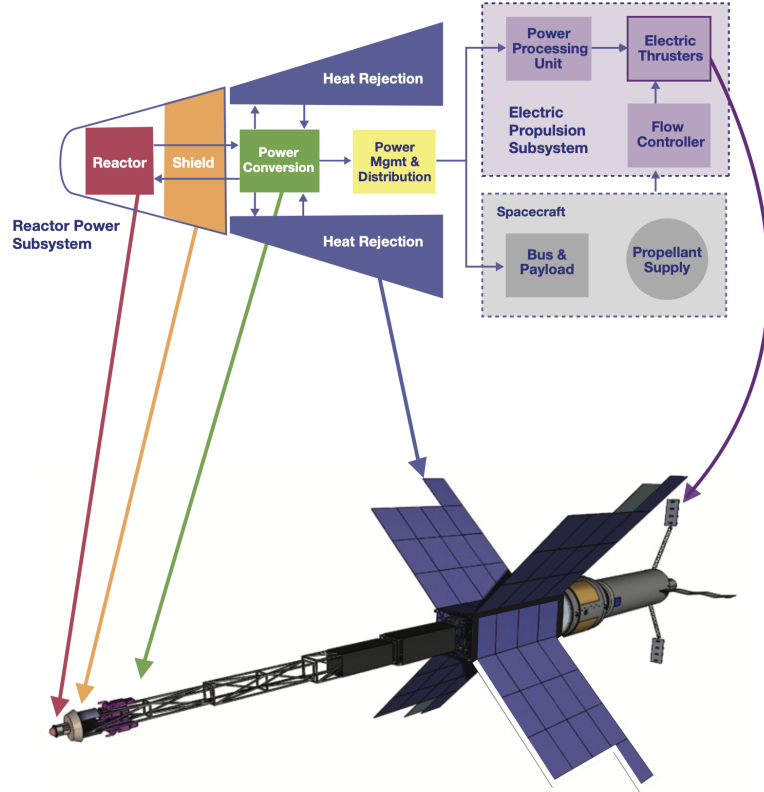


Figure 2.3: Nuclear Electric Propulsion system diagram [3].

Figure 2.3 shows a high-level schematic of an NEP system which can be broken down into six major components: a reactor (similar to NTP), a shield (also similar to NTP), a power conversion system, a heat rejection system, a power management and distribution (PMAD) subsystem, and an electrical propulsion (EP) subsystem, which consists of a power processing unit (PPU), a propellant management system (PMS) and thrusters. This outline will focus on the EP subsystem and its components, as this is where thrust generation occurs and where there is arguably the highest variability among system concepts due to the differences between thruster and propellant types. The 2021 National Academies of Sciences, Engineering, and Medicine (NASEM) study on space nuclear propulsion states that

NEP system performance is governed by the total system mass required to produce the required power level (i.e., the system specific mass, in kilograms per kilowatt-electric), the performance of the EP subsystem, and the lifetime and reliability of all subsystems. System design trades focus on maximizing the power conversion subsystem efficiency, the waste heat rejection temperature, and the efficiency and specific impulse (I_{sp}) of the EP subsystem while achieving the mission lifetime and reliability requirements. [17].

Because NEP systems generate high specific impulse but low thrust, such a system would need to be used in tandem with a chemical propulsion system for trajectory stages that require high thrust—primarily the planetary launch stages. Additionally, the use of NEP for the baseline mission would likely require the aggregate use of multiple NEP modules or subsystems to achieve greater propulsive power. Both of these facts should be regarded as complicating factors, but not necessarily limiting factors of NEP as a choice of propulsive system. Depending on mission architecture specifics, such as transit duration, NEP may provide advantages over NTP with regard to propellant and payload mass requirements and, in turn, mission cost factors. Table 2.1 shows the significant relative decrease in propellant mass in NEP systems compared to NTP, largely due to having greater propellant

efficiency. This is a significant advantage for longer-duration missions, where payload mass requirements are inevitably greater and will need to take up a greater proportion of the total initial mass.

2.3.1 NEP Fuel and Propellant Options

Although NEP systems are expected to use nuclear fuels similar to those in NTP systems to power their reactor subsystems, primarily high-assay low-enriched uranium (HALEU) and highly rich uranium (HEU), as discussed in Section 2.2.1, the propellants used for thrust generation in NEP systems differ significantly.

Xenon is the most commonly used propellant for current electric propulsion systems because of its high atomic mass, low ionization energy, and chemical inertness. These properties make xenon highly efficient for ionization and acceleration in electric thrusters, resulting in high specific impulses and relatively low system complexity. Furthermore, xenon's high density under pressure allows for efficient storage in spacecraft tanks. The primary drawback of xenon is its high cost and rarity.

Krypton is a cheaper alternative to xenon. Although krypton has a lower atomic mass and higher ionization energy than xenon, resulting in somewhat lower thrust efficiency, it is substantially more abundant and less expensive. Recent technological developments have improved the feasibility of krypton-fueled electric propulsion systems, particularly for missions where cost constraints outweigh the need for maximum propulsion efficiency.

Both xenon and krypton propellants offer long operational lifetimes, a crucial factor for deep-space missions where maintenance and resupply are impossible. The choice between them typically involves a trade-off between performance and cost, with xenon preferred for high-performance missions and krypton considered for missions prioritizing economy. Given the high stakes (human cost, predominantly) associated with the technical and operational challenges posed by a crewed Mars mission, xenon is the more likely choice for the propellant in an NEP system in this context.

2.3.2 EP Thrusters

In an NEP system, the electricity generated by a nuclear reactor is used to power electric thrusters. The two main types of electric thruster considered for space exploration missions are Hall-effect thrusters and ion thrusters.

Hall effect thrusters, used in the Psyche spacecraft [29], operate by using an electric field to accelerate ions, while a magnetic field perpendicular to the electric field confines and controls the motion of electrons. This combination creates a plasma that is expelled at high velocity to produce thrust. Hall thrusters are known for their relatively high thrust-to-power ratio compared to other electric propulsion systems, making them suitable for missions that require moderate thrust over long durations. They are robust, have a high operational lifetime and can achieve specific impulses typically in the range of 1500 to 3000 s.

Ion thrusters work by electrostatically accelerating ions using grids charged to high voltages. These systems achieve even higher specific impulses than Hall thrusters, often in the range of 3000 to 10,000 s, depending on the design and operating conditions. Ion thrusters provide very high propulsion efficiency but generate low levels of thrust, making them ideal for missions where gradual acceleration over extended periods is acceptable (longer-duration missions) [17].

Both types of thrusters are well suited to NEP applications, where continuous low-thrust operation over months or years can efficiently achieve the large velocity changes needed for deep space missions. The choice between Hall effect and ion thrusters depends on mission-specific factors such as desired transit time, spacecraft mass, available reactor power, and thrust efficiency requirements.

2.4 Comparison of NEP and NTP

Although NTP and NEP both use a nuclear reactor to generate heat energy, there are clear systematic differences in how each system ultimately produces thrust, and these lead to

significant differences in how that thrust can be used in a mission. Table 2.1 shows a direct comparison of estimated characteristics for both types of propulsion system.

Table 2.1 presents a comparison of estimated characteristics for NTP and NEP systems. While some attributes, such as specific impulse and operational lifetime, are directly comparable between the two propulsion types, others are more specific to each system. For example, the propellant mass flow rate (\dot{m}) directly influences thrust generation in NTP, as the exhaust velocity (v_e), which determines thrust, is driven by the acceleration of propellant through the nozzle. As discussed earlier, because NEP systems convert nuclear energy to electric power, the mass flow rate does not have the same impact on thrust.

Similarly, the value of F_{Earth} , or the engine's thrust under Earth gravity, is included to highlight the significant difference in magnitude between NTP and NEP propulsion. Although an individual electric propulsion (EP) thruster produces very low thrust, an NEP system would consist of a large array of such thrusters operating in parallel. The number of thrusters can vary widely depending on mission design, but the total thrust scales with both the number of thrusters and the available electrical power. Because NEP systems require megawatt-scale electrical power to achieve mission required thrust levels which have not yet been demonstrated in space, the power values presented in Table 2.1 should be interpreted as projected mission requirements rather than currently achievable power levels.⁴

To summarize the differences between NTP and NEP: NTP produces high thrust over relatively short burn periods, whereas NEP provides low, continuous thrust over extended durations. Intuitively, this suggests that NTP may be better suited for shorter-duration missions, which can accommodate the greater propellant fractions required by its lower fuel efficiency, while NEP may be more advantageous for longer missions where gradual acceleration is permissible and lower propellant mass fractions are feasible. The next chapter will examine whether these intuitions hold across different trajectory options.

⁴As discussed in the 2021 National Academies report on *Space Nuclear Propulsion*, while megawatt-class NEP systems are being studied, no such systems have yet been flown or validated in space.

Characteristic	Description	NTP	NEP
I_{sp}	Specific Impulse – a measure of time (in seconds) for which thrust is produced per unit of propellant per unit of gravitational force. Intuitively, it is the efficiency of propellant usage.	~ 900 s	1800 – 6000 s [4]
\dot{m}	Mass Flow Rate – the rate of propellant expulsion (in terms of thrust generation, this is relevant to NTP but not NEP)	~ 3.5 $\frac{\text{kg}}{\text{s}}$ [30]	–
F_{Earth}	Approximate magnitude of forward force on Earth ($F_{NTP} = I_{sp} \cdot \dot{m} \cdot g_0$ & $F_{NEP} = \frac{2 \cdot P \cdot \eta}{I_{sp} \cdot g_0}$)	~ 30,900 N	~ 170 – 560 N
Propellant Type	Type of propellant used to generate thrust	LH2-LOX	Xenon
PMF	Propellant Mass Fraction (fraction of initial spacecraft mass given by propellant $\frac{M_p}{M_i}$)	≈ 0.69*	≈ 0.35**
Power	Power available to EP thrusters	–	5.0 MWe
α ($\frac{\text{kg}}{\text{kWe}}$)	Specific Mass (ratio between the propulsion system mass to power generated) [31]	–	≤ 20 kg/kWe [17]
η	Thruster efficiency (EP)	–	~ 70%
Engine Structural Mass (kg)	Dry mass of engine system	2,000–10,000 kg	10,000–15,000 kg
Total Operational Lifetime	Time engine is capable of generating thrust, based on both reactor lifetime and power availability (thrust is generated intermittently in NTP and continuously in NEP)	~ 4 h	~ 1 – 2 yrs [17]

Table 2.1: Comparison of Estimated Characteristics for NTP and NEP

*Average of three element-level NTP configurations (core stage, in-line tank, and saddle truss with drop tank) from the 2037 NASA DRA 5.0 concept study. These represent conservative system-level PMFs that include tank, engine, and structural components.

**Estimated propellant masses (including both electric propulsion and chemical components) for an NEP conjunction-class mission, based on the NASA DRA 5.0 concept study.

Chapter 3

Trajectory Modeling & Mission Architecture Analysis

3.1 Introduction: Trajectory Types

In mission planning, trajectory design and the associated mission sequence, consisting of launch times, transit durations, and surface stay, exert the greatest influence on all other mission requirements, from mass to propulsion needs. These requirements are inherently tied to the chosen trajectory and mission sequence, making them crucial considerations in the development of space propulsion technologies. The timing and duration of the trajectory directly impact the mission's thrust requirements, and given the difference between NTP and NEP concerning this discussed in Chapter 2, trajectory decisions may illuminate which option is more appropriate.

There are many possible trajectories from Earth to Mars, with large variations in overall mission ΔV and duration—to the first order, these are the two competing variables which need to be optimized based on the need to minimize crew health risks associated with space exposure yet ensure sufficient time to achieve mission objectives. There are two main classifications of missions, determined largely by the planetary alignment of Earth and Mars

at the time of launch, and the surface duration which the trajectory enables. Conjunction-class missions are commonly referred to as “long-stay,” and generally correspond to longer overall mission duration (usually around 900 days) and surface stay (up to 500 days), but lower mission ΔV . Opposition-class missions, commonly called “short-stay,” typically have shorter overall mission and surface durations (30 to 90 days and 500 to 650 days respectively), but higher overall ΔV [4].

While both mission types are designed on the principle of minimizing ΔV in the choice of launch time, opposition-class missions depart from this in order to reduce mission duration, while conjunction-class missions generally seek to maintain this minimum. These missions more closely resemble the Hohmann transfer trajectory outlined in 1.2.1. (For reasons explained previously, a true Hohmann transfer between Earth and Mars is not possible, but the principles underlying this idealized trajectory can be applied in determining maximally energy-efficient launch windows.) In order to minimize ΔV , these missions require a longer surface stay to enable symmetric outbound and inbound trajectories. This symmetry is observable in 3.1, which illustrates examples of typical opposition and conjunction missions.

Opposition-class missions, in contrast, are more likely to utilize nonsymmetric outbound and inbound trajectories and are less constrained by inbound launch timing and surface stay for this reason. Similarly, these trajectories are usually shorter with greater ΔV s due to an exponential relationship between ΔV and transit duration. Because of this relationship, opposition-class missions are frequently excluded from consideration in mission analysis.

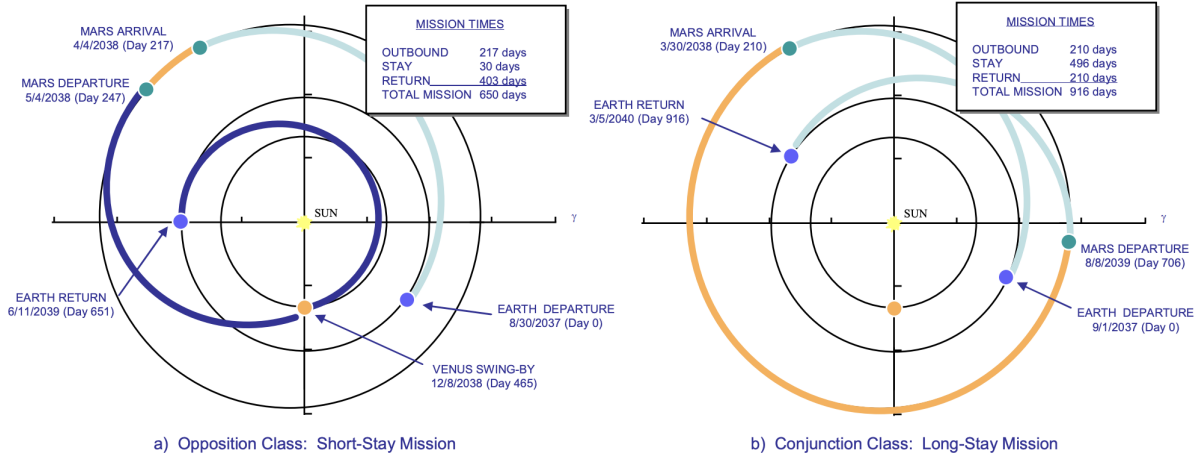


Figure 3.1: A comparison of two possible trajectories representative of conjunction- and opposition- class missions. [4].

In the context of the baseline crewed mission to Mars, it is not obvious which of these mission architectures is favorable, and strong arguments have been made for both. The Human Exploration of Mars Design Reference Architecture 5.0 (DRA 5.0) maintains that a long-stay, conjunction-class mission is necessary to enable sufficient surface exploration and maximize science return, key priorities of the mission, and a 30-day stay simply is not enough. It reasoned that short-stay human surface missions could not make the best use of mobility to optimally explore a region due to the time available for extravehicular activity (EVA) (including subsurface access system operations, such as a deep drilling), and that these missions “do not optimize the ‘iteration cycle time’ that is associated with in-situ field investigations on the basis of time available (i.e., that are too few cycles in which to adapt to the unexpected scientific context that is likely to emerge). Short-stay human surface missions do not allow time for sample high-grading to ensure a best subset of materials is returned for detailed analysis on Earth. This limits the discovery potential that is intrinsic to field sampling.” [4]

On the other hand, a 2014 study by the American Institute of Aeronautics and Astronautics argues that there are unresolved drawbacks to conjunction-class missions, primarily, the long duration of the mission, often reaching 1000 days or more, and the greater invariability

of these durations expose the crew to greater health risks, a mission variable with high uncertainty and gross contingency. Additionally, they argue that the rejection of opposition-class missions on the basis of having greater ΔV is premature, with the application of the rocket equation being an oversimplification of the relationship between ΔV and propellant mass (or the payload mass ratio, of which propellant mass is a crucial part, in the case of 1.3), stating that “Short stay trajectories are intrinsically non-symmetric with larger ΔV investments required for a single leg of the mission. This presents an added complexity in determining the trajectory, but also provides opportunities to optimize ΔV expenditure across the mission.” So, for opposition-class missions, in which the ΔV budget is split into more burns over the duration of each transit, it is possible to be more strategic by concentrating fuel expenditure into phases in which the propulsive mass is the smallest (that is, it has a much faster inbound journey than outbound) [32]. Although certain legs of the opposition-class trajectory may be highly energy-inefficient, having such concentrations of ΔV may enable other sections of the trajectory to be more efficient, balancing out the overall trajectory. Therefore, while there is no departure from the relationship between ΔV and the payload mass ratio in the opposition-class scenario, this relationship should be regarded with greater nuance and more careful analysis may be required to determine possible opposition class trajectories.

3.2 Trajectory Modeling

This section presents trajectory modeling performed in Python and subsequent analysis to constrain mission architecture requirements including launch windows and corresponding minimum ΔV trajectories for conjunction- and opposition-class scenarios. It also explores how such mission architecture analyses may inform the requirements of a nuclear propulsion system, and offers a verdict regarding which type of nuclear propulsion (NTP or NEP) may be appropriate for each category of mission architecture.

The trajectory modeling presented here uses Poliastro[33], a Python library for astrodynamics and orbital mechanics¹. To retrieve ephemerides for solar system bodies, that is, the celestial coordinates giving their positions at any given time (based on parameters such as orbital inclination and eccentricity), Polisastro uses two databases from Jet Propulsion Laboratory (JPL): the Small-Body Database (SDBS) and Horizons².

To solve for the trajectory between two celestial bodies based on these data, Poliastro contains a Lambert problem solver. Given the boundary conditions of flight time (Δt) and two positions \vec{r}_0 and \vec{r}_f , the Lambert's problem solves for the orbit between them. The orbit could be elliptical, parabolic, or hyperbolic depending on the values of the positions and the flight time, and the solution requires solving a set of transcendental equations derived from Kepler's laws of planetary motion. [34][35]. The trajectory plots shown in this Chapter were produced using this technique.

3.2.1 Identifying Launch Windows: Preliminary ΔV and Trajectory Plots

The first step in determining an ideal trajectory is to determine launch opportunities, which are given when the two planets are in a configuration that minimizes ΔV . The approach taken here was to plot the total mission ΔV for a hypothetical mission architecture for different dates (see Figure 3.2)—the minima of this plot show the launch dates which correspond to a minimum ΔV for the constant mission architecture constraints.

The date range from early 2037 to late 2041 was selected based on the identification of 2039 as a target launch window by NASA and the Space Nuclear Propulsion Technologies Committee of the National Academies of Sciences, Engineering, and Medicine [17]. Figures 3.2 and 3.3 support this assessment by confirming the presence of a favorable launch

¹For more information, see the Poliastro documentation: <https://docs.poliastro.space/en/stable/>.

²See the JPL Small-Body Database (SBDB) at https://ssd.jpl.nasa.gov/tools/sbdb_lookup.html#/ and the JPL Horizons system at <https://ssd.jpl.nasa.gov/horizons/>.

opportunity in 2039.

Figure 3.2 is based on a generalized mission architecture with a 40-day surface stay and symmetric outbound and return trajectories. Each curve represents a different total transit duration. While such generalizations are useful for broad analysis, they do not necessarily reflect the structure of realistic conjunction- or opposition-class missions. In a conjunction mission, for instance, the surface duration would typically be longer, while opposition missions would likely involve asymmetric transit times. However, this simplified architecture remains valuable for visualizing the periodic behavior of total mission ΔV , resulting from the synodic cycle of the planets, and for identifying approximate launch windows for continued analysis.

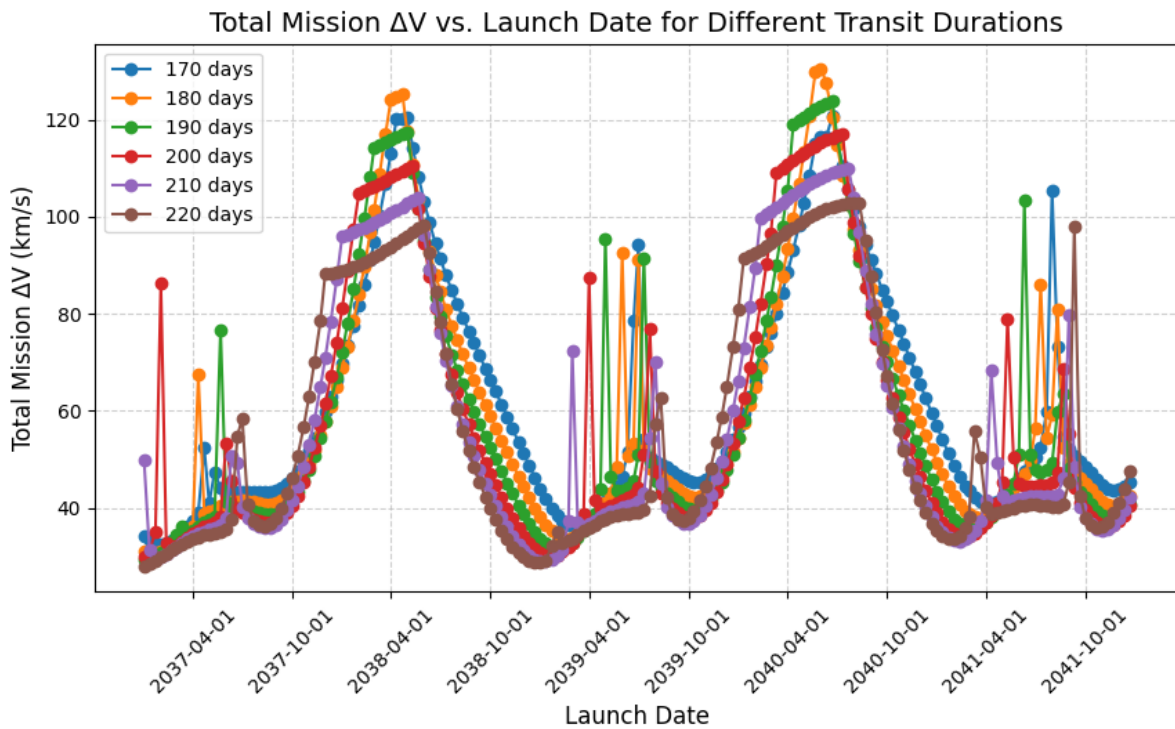


Figure 3.2: A plot of total mission ΔV (outbound & inbound) vs. launch date for the following transit durations: 170 days (blue), 180 days (yellow), 190 days (green), 200 days (red), 210 days (purple), 220 days (brown). Launch dates span from January 2037 to October 2041 and occur on the 1st, 10th, and 22nd of each month. The missions shown here have symmetric outbound and inbound trajectories and a Mars surface duration of 40 days.

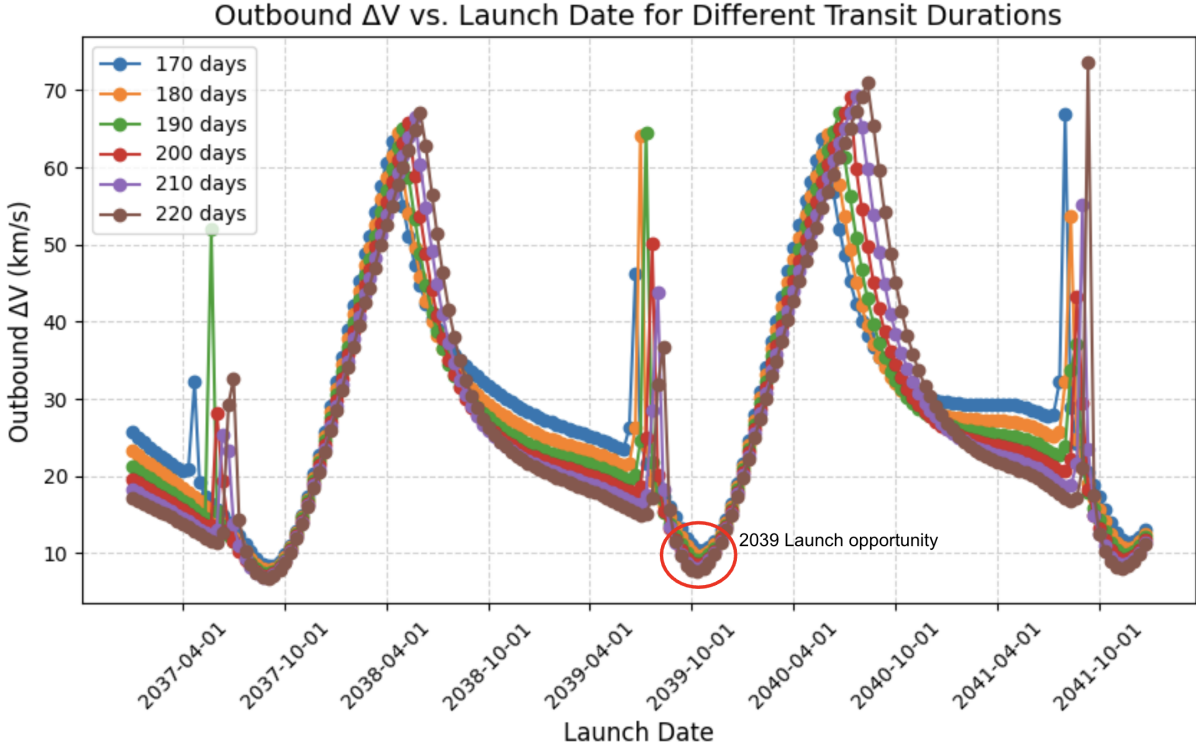


Figure 3.3: A plot of outbound ΔV vs. launch date for the following transit durations: 170 days (blue), 180 days (yellow), 190 days (green), 200 days (red), 210 days (purple), 220 days (brown). Launch dates span from January 2037 to October 2041 and occur on the 1st, 10th, and 22nd of each month. Launch opportunities are considered to be the ΔV troughs. This plot shows 3 possible launch windows occurring in 2037, 2039, and 2041. The 2039 launch window is circled and examined in subsequent analysis.

Removing some of the mission generalizations in Figure 3.2, Figure 3.3 shows just the outbound ΔV for the same launch dates, date range, and transit durations. There is a slight shift in the launch window, emphasizing the importance of surface duration and return launch date in trajectory optimization. During the launch windows (i.e., the ΔV troughs), variation in the ΔV for different transit durations is relatively low, indicating greater launch-date flexibility within these low ΔV periods. Although distinct launch windows are also visible in 2037 and 2041, the 2039 opportunity was selected for further analysis because of its alignment with NASA's prior mission planning. Furthermore, while the 2037 opportunity offers a slight advantage in ΔV minimization as a global minimum in this timeframe, it is unlikely to be feasible given the current state of technology readiness.

This plot also shows the feature of longer transit durations occasionally corresponding to greater overall ΔV values—particularly around the peaks of the curves—a feature that is actually more articulated when isolating the outbound journey. To better understand this phenomenon, it is important to understand the type of trajectory that would occur for the planetary configuration at these launch dates. Figure 3.4 shows a visualization of the outbound trajectory during the first ΔV peak for a launch date of June 1, 2038. On this date, the planets are in direct opposition, which means that Mars is radially outward from Earth. This geometry demands a transfer orbit with such high eccentricity that it is essentially a straight shot. This is a high-energy maneuver that directly opposes the energy efficiency of the Hohmann transfer (1.2.1). Due to the distance-minimizing aspect of this trajectory, performing the maneuver in a greater amount of time actually corresponds to a greater energy maneuver. Correspondingly, the ΔV dips in both plots reflect the conjunction configuration of Earth and Mars, which most closely resembles the Hohmann transfer trajectory.

A feature of both ΔV plots to be addressed is that for certain launch dates, shorter transit durations appear to result in greater overall ΔV values, mainly at the peaks of the curves. This is explained by considering the fact that Earth and Mars are in close opposition during these periods, requiring hyperbolic trajectories such as the one in Figure 3.4, for which shorter transit durations are actually more efficient.

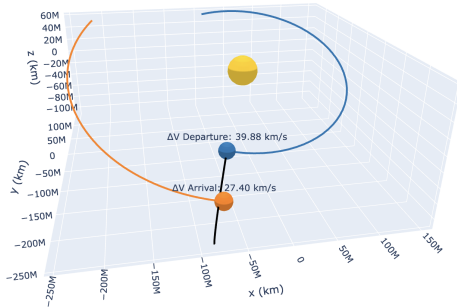


Figure 3.4: A sample plot of the hyperbolic trajectory corresponding to the first ΔV peak, a local maximum, in 3.3 with a launch date of June 1, 2038 and a Mars arrival date of January 7, 2039 (a 220-day transit). The total ΔV for this 2-burn outbound trajectory is 67.8 km/s, a maximum with respect to other possible launch dates, and highly nonoptimal trajectory choice.

Both plots exhibit sharp ΔV spikes, primarily between peaks. These anomalies are most likely caused either by failures of the Lambert solver due to numerical instabilities or gravitational perturbations due to other celestial bodies such as the Moon, Martian moons, or asteroids. In the case of the former, possibly incongruences between the given time-of-flight (TOF) and aspects of the orbital geometry, such as the transfer angle being too large or small, can cause convergence issues in the iterative process of the Lambert solver. Notice that the solver fails at regular intervals in the synodic period, consistently in the ΔV troughs right before the minima. The fact that these anomalies are periodic indicates this type of failure, as gravitational perturbations from other bodies would not be tied to the Earth-Mars synodic period.

3.2.2 Optimizing Transit Duration and ΔV

With a launch window identified based on ΔV variations, the next step is to isolate specific trajectories that balance transit duration and ΔV . Because these parameters are interdependent, there is an inevitable trade-off: greater ΔV allows for shorter transit times, minimizing crew health risk and allowing for greater surface duration, but demanding greater propulsive capabilities if overall mission duration is to be controlled. Conversely, minimizing ΔV and using a longer transit duration reduces propulsive needs but leads to longer mission durations, increasing operational and biological concerns.

This analysis examines the relationship and trade-off between transit duration and ΔV within the 2039 launch window. By identifying trajectories that exhibit reasonable balances between these two parameters, the corresponding propulsive requirements (I_{sp} and thrust) can reveal whether there is an obvious trajectory dependence in the choice between NEP and NTP and ultimately whether one type of propulsion is more viable for human Mars exploration.

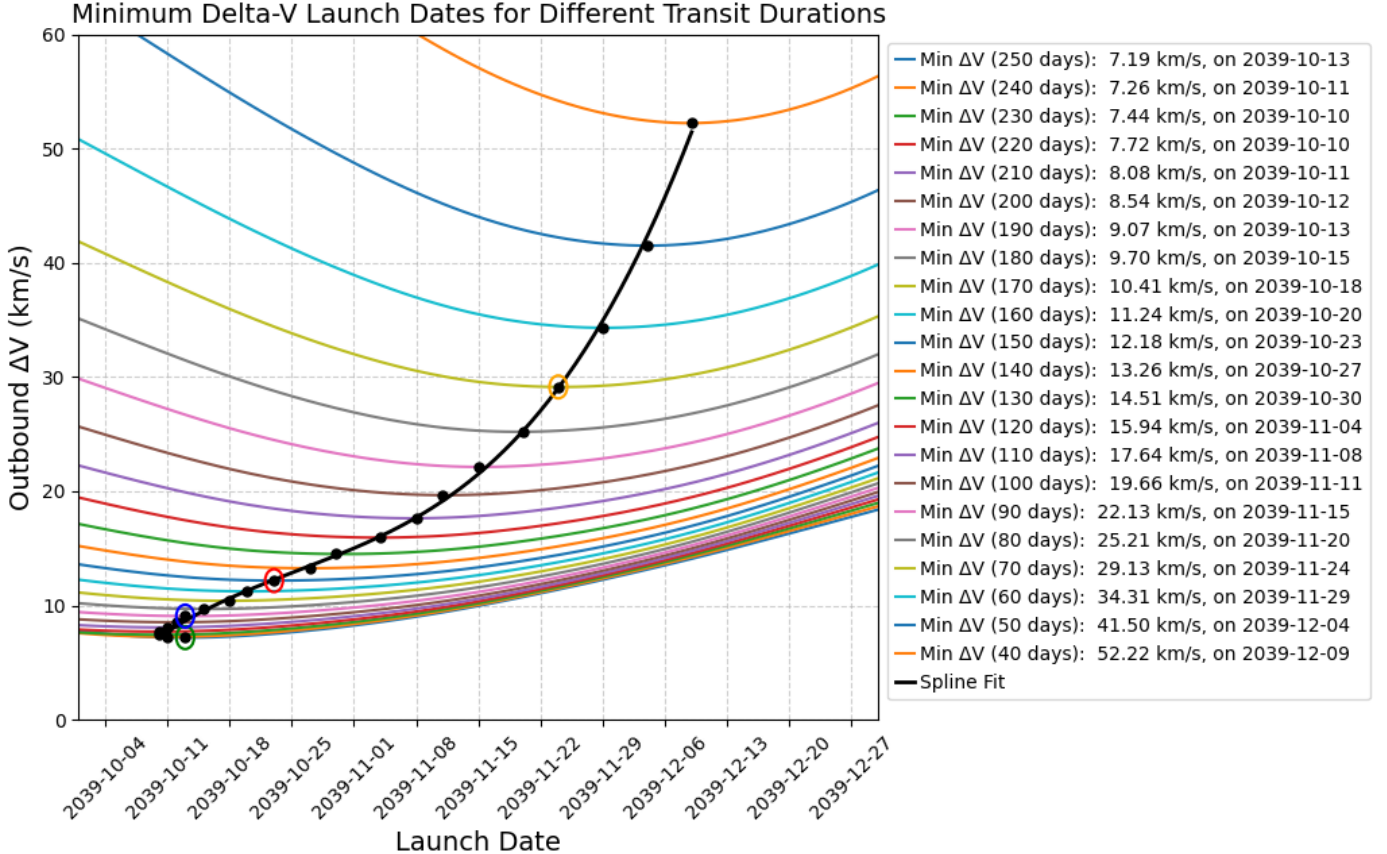


Figure 3.5: A closer look at the 2039 launch window: Launch date vs. minimum outbound ΔV for a range of dates in Autumn 2039. The contours represent the change in outbound ΔV over time for different transit durations, as in Figure 3.3. The black data points represent minimum ΔV values for each transit duration, and are fitted with a piecewise polynomial (spline) curve. Although the shorter transit durations may not be technically feasible, they are included in this plot to demonstrate the ΔV magnitudes they require. This plot demonstrates an optimization tradeoff between ΔV , transit duration, and launch date. The circled data points correspond to trajectories shown in Figure 3.7, and are color-coded. The green circle shows the global-minimum ΔV conjunction-class trajectory (250 days) for all trajectories in the launch window, including ones with transit durations greater than 250 days. The orange circle shows an example of an infeasible trajectory with excessive ΔV . The red and blue circles show possible opposition-class trajectories, selected based on the relationship shown in Figure 3.6.

Figure 3.5 shows the minimum ΔV values for various transit durations (represented by each contour) in the 2039 launch window identified in Figure 3.3. Note that in this launch window, conjunction- and opposition- class missions are not distinguished based on launch time and planetary alignment, but rather on transit duration (with a maximum cutoff of

approximately 170 days for opposition-class missions).

This plot has two purposes: first, to visualize the relationship between ΔV , transit duration, and launch date. The nonlinearity of the main curve reveals an optimization trade-off between these three variables. Secondarily, this plot allows identification of the launch date which minimizes ΔV for each transit duration. Notably, the data is best represented by a piecewise polynomial (spline) curve, but qualitatively resemble an exponential trend—Figure 3.6 reveals that there is an exponential relationship between changes in ΔV and changes in transit duration. This suggests that certain reductions in transit durations may require disproportionately large increases in ΔV . For instance, a transit duration decrease from 220 to 210 days corresponds to a ΔV increase of approximately 0.3 km/s, while a transit duration decrease from 120 to 110 days corresponds to a ΔV increase of approximately 2 km/s, which would create a significantly larger fuel requirement. However, the point at which this ΔV increase becomes prohibitive is not immediately obvious and requires further investigation.

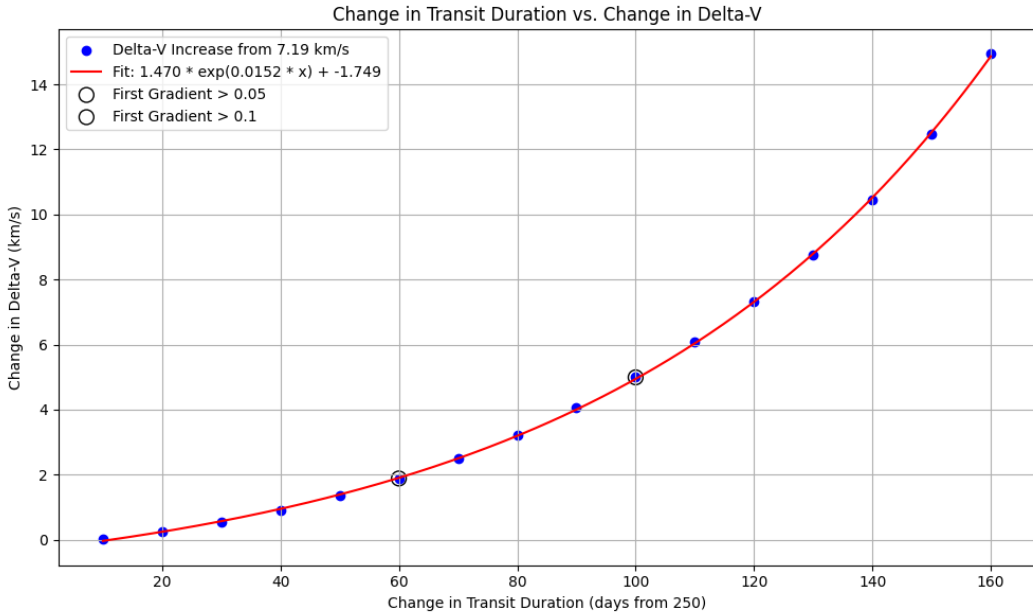


Figure 3.6: Plot showing the exponential relationship between decreases in transit duration and ΔV . Circled data points correspond to where slope exceeds 0.05 and 0.1, based on suggested ratios to identify opposition-class trajectories. The corresponding transit durations for these data points are 190 days and 150 days.

The relative cost of increased ΔV or longer transit durations depends on a multitude of mission-specific factors, including crew health risks from prolonged space exposure, propellant and payload mass constraints, and surface time required to meet scientific objectives. Although these trade-offs are ultimately quantifiable, the definition of precise cost functions for each variable is beyond the scope of this thesis. Therefore, a simplified decision is adopted to allow further analysis, with the understanding that more detailed optimization could be pursued in future work.

Figure 3.6, an alternative form of the data in Figure 3.5, shows the exponential relationship between changes in ΔV and changes in transit duration. The circled points point to where the slope exceeds 0.05 and 0.10 respectively, which was used to identify opposition-class trajectories with these ΔV -transit-duration ratios—plots for which are shown in Figure 3.7. The thresholds were selected on the basis that slopes of 0.1 and 0.05 mean that small reductions in transit time still result in relatively small penalties ΔV (10% and 5%, respectively). However, this selection ultimately relied on qualitative judgment and was therefore somewhat arbitrary. Continued work could refine these values by quantifying the economic, physiological, and other costs associated with longer transits and greater overall ΔV .

Having identified these optimal outbound launch dates and transit durations, the next step is to design an optimal inbound trajectory and surface duration. For conjunction class missions, we determine the surface duration which allows for a symmetric inbound trajectory which also minimizes ΔV . For opposition class missions, much more experimentation is required to identify optimal trajectories, since these missions depart from the ΔV minimization principle. The two opposition-class trajectories identified in Figures 3.6 and 3.7 may optimize ΔV for their respective transit durations, however, factoring in surface duration and inbound transit possibilities leads to great variation in round-trip ΔV for these missions, which will be explored in section 3.4.

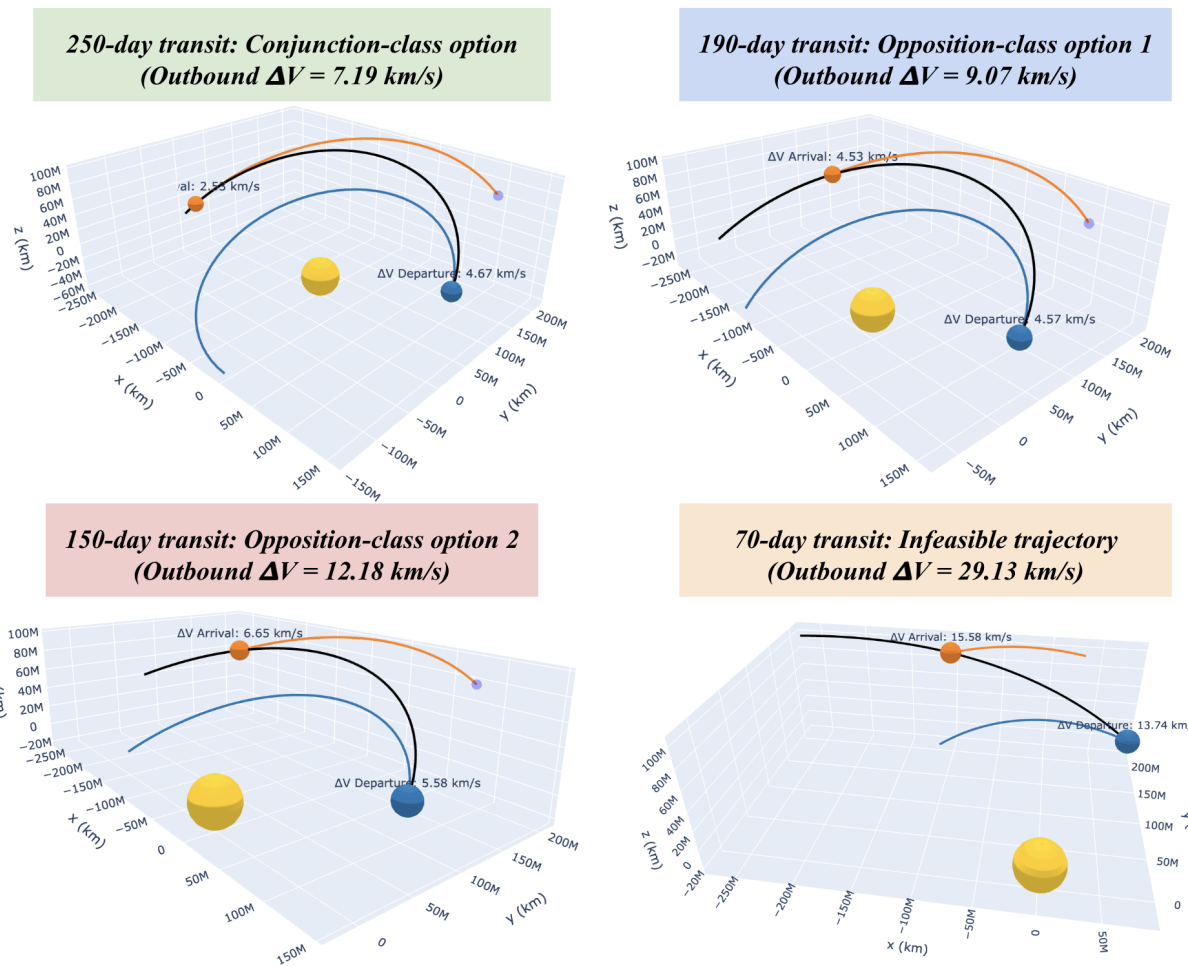


Figure 3.7: A comparison of trajectory options corresponding to the circle data-points in Figure 3.5, color matched. The top left image shows the identified conjunction-class option, the global minimum ΔV trajectory within the 2039 launch window with a 250-day outbound transit. The bottom right shows an example of an infeasible trajectory with a very short transit duration (70 days) and very high ΔV (29.13 km/s). The top right and bottom left images show intermediate ΔV opposition-class trajectories (190 and 150 days respectively), identified using slope thresholds in Figure 3.6.

3.3 Conjunction-Class Mission Analysis

With the primary advantage of conjunction-class missions being its ΔV minimization, the principle associated with conjunction-class trajectory design is adhering with this minimization. As explained previously, this is why conjunction-class missions show symmetric inbound and outbound trajectories, so that both interplanetary transfers are as close as

possible to the maximally efficient Hohmann transfer.

The NASA Design Reference Architecture 5.0 (DRA 5.0) estimates a surface duration of 496 days for conjunction-class mission, seen in Figure 3.1 [4]. Using the exact same transit duration for the outbound and inbound trajectories, the surface duration which minimizes ΔV is 494 days—in line with this NASA estimate. However, the total ΔV for both transits using this mission architecture is high for conjunction-class, at 18.33 km/s.

Using the method previously used to calculate optimal launch dates that minimize ΔV , the surface duration and inbound transit duration that minimize ΔV were calculated to be 421 days and 295 days, respectively, resulting in an inbound ΔV of just 6.33 km/s; less than this mission’s outbound ΔV of 7.2 km/s. The round-trip total, and the minimum calculated ΔV in the 2039 launch window, is 13.53 km/s—excluding the planetary launch and descent stages.

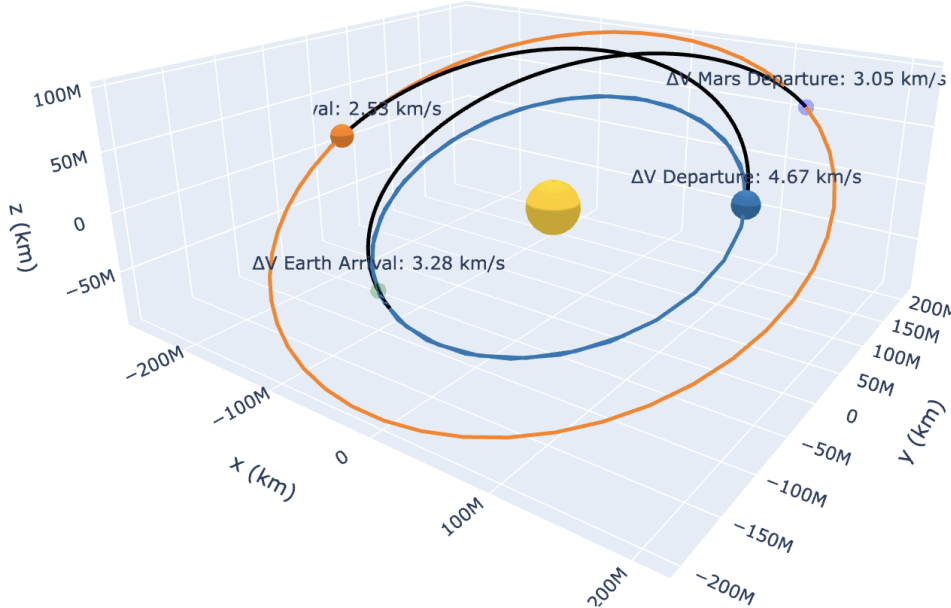


Figure 3.8: The trajectory plot for the conjunction-class mission chosen for analysis of propulsive requirements, with the minimum calculated ΔV in the 2039 launch window. The outbound ΔV and transit duration are 7.2 km/s and 250 days, the surface duration is 421 days, and the inbound ΔV and transit duration are 6.33 km/s and 295 days. This gives a total mission duration of 966 days and a round-trip ΔV of 13.53 km/s, excluding launch and descent stages.

Based on the Tsiolkovsky rocket equation (1.3) and using an initial-to-final mass ratio ($\frac{m_0}{m_f}$) of 2.395 derived from the mass breakdown of DRA 5.0 for a possible mission using nuclear thermal propulsion [4], the specific impulse (I_{sp}) required to complete both transfers is calculated to be 1544 s, which exceeds the typical capabilities of NTP systems, whose specific impulses generally do not exceed 900 s.

This does not definitively rule out NTP as an option for this mission, however, since greater mass ratios bring the specific impulse within the operational range of NTP designs. Increasing the mass ratio to 4.5, or essentially doubling the amount of propellant, reduces the I_{sp} requirement to 896 s, which is commensurate with the performance of engines in the NERVA program over 50 years ago. Given that most I_{sp} estimates for NTP systems are based on the results of the NERVA program, it is possible that modern NTP reactor and engine designs may provide even greater I_{sp} . However, increasing the propellant mass to this extent would have significant implications for the mission architecture, particularly for the launch stage.

In the case of long-duration conjunction-class missions such as this, higher propellant mass ratios (on the order of 3 or more) are less likely to be feasible, since these missions have greater payload requirements. These missions demand a substantial payload for life support, crew, and scientific equipment, and increasing the propellant mass to such an extent could lead to an impractical increase in spacecraft size and launch vehicle requirements. Ultimately, the feasibility of NTP for this particular mission has precarious certainty. Although higher initial-to-final mass ratios and modern reactor and engine designs with greater than typical I_{sp} capabilities possibly align NTP with the propulsive requirements of this mission, they would not allow for a conservative mission design. The proximity of NTP's capabilities to the minimum propulsion requirements of the mission suggests that relying on NTP could introduce unnecessary complexity and risk.

For NEP, comparative mass breakdowns for theoretical missions (compared to those provided in DRA 5.0) were not readily available. However, we can derive an approximate

mass ratio from the propellant mass fractions provided in Table 2.1, which show a value of 0.69 for NTP and 0.35 for NEP. Given that the final mass of the system is approximately the initial mass minus the propellant mass, we can approximate the mass ratio for NEP as follows. If 35% of the initial mass is propellant, the remaining 65% is the final mass. Thus, the mass ratio for NEP is:

$$\frac{m_0}{m_f} = \frac{1}{0.65} = 1.538 \quad (3.1)$$

This lower mass ratio relative to NTP (2.395) is expected, as NEP systems rely on electrical energy storage and expel less propellant over the course of a mission. Applying this ratio to the Tsiolkovsky rocket equation, the specific impulse required of an NEP system for this mission is calculated to be 3132 s, which falls neatly within the range of possible NEP I_{sp} values (1800 - 6000 s, as in table 2.1). Although the NEP calculated mass ratio is highly approximate, significant corrections to this value due to limitations of this analysis are likely to still result in I_{sp} values within the required range.

There are some limitations to this analysis that limit the conclusiveness of the feasibility of the use of NTP or NEP in conjunction-class missions. Although this mission provided the minimum calculated ΔV in this particular analysis, there is no certainty that other mission architectures for conjunction-class missions may not provide even lower round-trip ΔV for launch times, in the identified 2039 launch window or otherwise. Additionally, since the trajectory modeling code does not account for launch or descent stages, accounting for this stage would significantly increase the propulsion demands for an NTP system such that even doubling the propellant mass may not be sufficient.

On the other hand, because the trajectory design approach here only considers propulsive orbital insertions and does not consider aeroassist or aerobraking techniques that may significantly decrease ΔV , there probably exist other conjunction-class mission architectures with significantly lower ΔV requirements. The following conclusions should be taken with these considerations in mind.

Overall, for this particular conjunction-class mission, which was calculated to have a minimum ΔV in the 2039 launch window, the analysis suggests that NEP can easily meet the mission's propulsive needs, allowing for a more conservative mission design. In contrast, NTP systems would require large propellant mass fractions that may not be feasible given the typical payload demands of conjunction-class missions. This finding supports the thesis that the choice between NEP and NTP is closely linked to trajectory-dependent propulsive requirements, which vary across different mission architectures. Moreover, it emphasizes that strategic mission planning requires the concurrent consideration of both mission architecture and propulsive technologies.

3.4 Opposition-Class Mission Analysis

Because opposition-class missions are not constrained by having surface durations which allow for maximally efficient inbound trajectories, there is much more variation involved in their design, and in their overall mission durations and ΔV s. The two opposition-trajectories chosen for analysis (Figure 3.9) have strikingly different characteristics: Option 1 is a very short round-trip mission (430 days) with a very high ΔV cost, and Option 2 is a longer mission (740 days) with a lower ΔV cost, although both significantly exceed the ΔV requirement of the selected conjunction-class mission.

Both missions use the 190-day optimal outbound trajectory identified using the ΔV -transit-duration ratio threshold in Figure 3.6, and a 30-day surface duration on Mars, which is typical for opposition-class missions. The inbound trajectories for Options 1 and 2 correspond to the first and second ΔV minima, respectively, for the Mars launch date determined by the 190-day outbound trajectory and the 30-day surface duration.

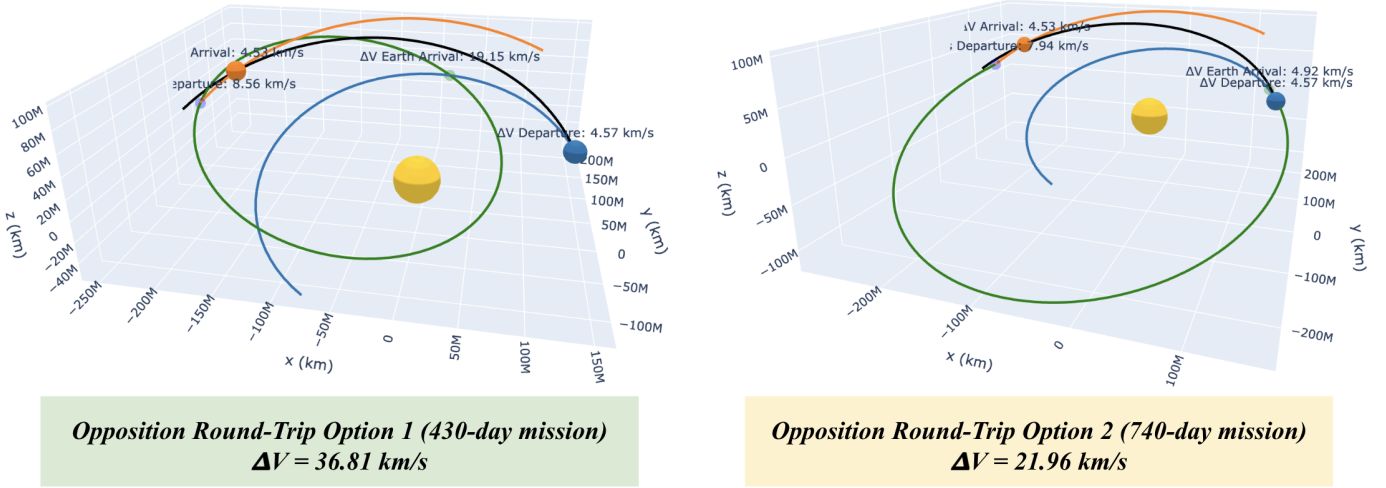


Figure 3.9: Two opposition-class trajectories: Option 1 is a short-duration, high ΔV (36.81 km/s) mission and Option 2 is a longer-duration, lower- ΔV (21.96 km/s) mission, which uses a long duration (520 days) inbound transit.

There are four scenarios to consider: one for each mission (Option 1 and Option 2) paired with each propulsion type (NTP and NEP). Table 3.1 shows each pairing with the initial-final mass ratio that brings the specific impulse (I_{sp}) within the range associated with each propulsion type. The feasibility rating in column 5 is attributed on the basis of whether that mass ratio is realistic for each propulsion type, where the conservative upper limits for NTP and NEP are considered to be roughly 5 and 2 respectively. These upper limits were chosen on the basis that in general, opposition-class missions enable greater propellant mass due to requiring less payload mass, justifying the extension of the mass ratios of 2.395 and 1.5 previously determined for the conjunction-class mission.

	ΔV (km/s)	Mass Ratio ($\frac{M_0}{M_f}$)	Required I_{sp} (s)	Feasibility Rating (1-4)
Option 1 with NEP	36.81	1.85	6099 s	2
Option 2 with NEP	21.96	1.5	5520.9 s	1
Option 1 with NTP	36.81	35.0	1055 s	4
Option 2 with NTP	21.96	8.5	1046 s	3

Table 3.1: Mass ratios and I_{sp} requirements for NTP and NEP under two opposition-class mission options. Feasibility ratings (1-4, with 1 being the most feasible) are attributed on the basis of whether these requirements align with allowed ranges (mass ratio ranges are approximated in this section and I_{sp} ranges are outlined in Table 2.1).

Based on these mass ratios and I_{sp} requirements, the feasibility of Option 1, the 430-day mission, seems unlikely—especially for NTP, where the calculated mass ratio that brings I_{sp} within an appropriate range (~ 1000 s) is 35. For both of these opposition-class trajectories, NEP outperforms NTP. This challenges the idea that NTP, because of its high thrust relative to NEP, is more suitable for short-duration missions.

Based on the calculated mass ratios and I_{sp} requirements, the feasibility of Option 1, the 430-day mission, appears unlikely, especially for NTP, where the calculated mass ratio needed to bring I_{sp} within a feasible range (approximately 1000 s) is 35. For both of these opposition-class trajectories, NEP outperforms NTP. This challenges the widely held view that NTP, due to its higher thrust relative to NEP, is generally more suitable for short-duration missions.

Despite this result, which seems to prohibit the use of NTP in shorter duration missions, it is not reasonable to generalize opposition-class missions based on these two possible missions. Given the nuance of opposition-class mission design and the variability of their trajectories, it is most likely that alternative opposition-class mission designs strike a more optimal balance between ΔV and mission duration than seen here. For instance, Borowski et al. outline a possible crewed opposition-class mission in 2033 that uses a pre-deployed Earth Return Vehicle (ERV) to bring the crew back to Earth [36]. This mission design results in

a total ΔV of ~ 9.85 km/s (even lower than the conjunction-class mission examined in 3.3), and a mission duration of 605 - 665 days, depending on whether a 21 day Phobos orbital rendezvous is included.

Although this mission design is certainly more complex in utilizing an auxiliary ERV to return the crew, which may have its own operational drawbacks, it only requires an initial-to-final mass ratio of 2.75 to bring the I_{sp} below 1000 s, making it well within the feasible range for NTP systems based on the Tsiolkovsky rocket equation. This example demonstrates that, with careful mission planning, NTP can indeed remain viable for certain opposition-class missions, despite the challenges identified in the two trajectory options initially considered.

From the extent of the NTP discussion in this thesis, it is difficult to define a strict upper limit for feasible initial-to-final mass ratios. Although the mass ratio of 8.5 calculated for NTP in Option 2 appears high, the significant reduction from Option 1 to Option 2 suggests that alternative opposition-class missions, particularly those with slightly lower ΔV requirements, may remain feasible for NTP systems.

Nevertheless, the results of this analysis indicate broader viability for NEP compared to NTP. For both Option 1 and Option 2, NEP provides mass ratios and specific impulse values within the outlined ranges of Table 2.1 and subsequent discussions. This analysis indicates that an NEP system can accommodate mission architectures with short or long transit durations and with a wide range of mission ΔV s (up to 37 km/s, excluding launch and descent stages, according to this analysis). Additionally, in both opposition- and conjunction-class analyses, NEP allows for greater conservatism in mission design because its I_{sp} and mass-ratio requirements consistently provide a larger operational buffer than those associated with NTP.

3.5 Final Thoughts

While the results of this analysis show that NEP may be feasible for a wider range of mission architectures, the crucial takeaway is this: In the interest of strategic planning for a crewed mission to Mars, the propulsive requirements associated with different mission architectures are a necessary factor. Although mission architectures with greater overall duration (conjunction-class missions) potentially allow for more exploration and science objectives to be met and reduce overall propulsive requirements, they are associated with higher operational and human risk. Conversely, shorter-duration (opposition-class) missions may reduce exploration capabilities and have greater propulsive needs, but allow for more conservative mission design and reduce these risks.

Based on these fundamental differences, the choice between NTP and NEP is elucidated. In particular, the consideration of investing in NTP development for a crewed Mars mission must acknowledge potential limitations in mission architecture options.

Building on this work, future research could refine the analysis by quantitatively assessing the costs associated with increased transit duration and ΔV requirements, considering economic, health, and mission success factors. Such studies could offer sharper insights into the trade-offs involved in designing opposition-class missions in particular, and further clarify the success of NTP and NEP in enabling human exploration of Mars.

Appendix A

NEP Synergies with Surface Power Generation

A possible advantage of nuclear electric propulsion (NEP) compared to nuclear thermal propulsion (NTP) is the potential dual use in the context of surface power generation—a technological requirement which also requires significant planning and development prior to the baseline mission and which has significant implications for payload mass.

A 2023 White Paper [37] part of NASA’s Moon to Mars project outlines several technologies, existing or in development, which can facilitate surface power generation for life support and ascent propellant manufacturing needs while considering the specific challenges imposed by the Martian environment. The surface power needs are dependent on the duration spent on the surface and the crew size—this can vary from 10 kilowatts of power for a 2 person crew staying for 30 days to megawatt class power systems in other architectures.

The White Paper argues that solar power will only be feasible if augmented with other technologies to combat challenges imposed by the Martian environment, including atmospheric dust and reduced solar flux (the maximum solar flux on Mars is only around 45 percent of solar flux experienced on the surface of Earth). For instance, dust wipers or electrodynamic dust removal could keep solar arrays clean and a mechanical array tilting

system could maximize exposure to sunlight. However, the highly likely scenario of a dust storm could cause excessive atmospheric dust that cannot be mitigated by these additional mechanisms. Additionally, Mars follows a day/night cycle similar to Earth, and so solar power cannot be generated at night. If a solar power system is used, it will need to include overnight energy storage capabilities.

Another proposed system is the use of fuel cells and Martian geothermal energy. These are unlikely systems for similar reasons, primarily due to their mass requirements. The former require the production of reactants that can use more energy and production mass than the fuel cells actually provide. In addition to utilizing heavy equipment, accessing geothermal energy is not feasible due to the time it would take to implement such a system and the constraint imposed by requiring proximity to geothermal sources. Given the frequent dust storms on Mars, the use of wind to generate power seems like a possibility. However, the Martian atmosphere is too thin to produce winds strong enough to generate power.

Nuclear power, including radioisotope power systems (as used on the Curiosity rover), and fission systems, provide the benefit of being unaffected by time of day and weather considerations as they are non-reliant on solar exposure. Fission surface power can also provide more power than radioisotope systems and thus may be a better option for life-support needs. This type of surface power generation system exhibits significant synergies with NEP, since both convert nuclear energy into electrical power for continuous use. NTP technologies do not share the same possible overlap since they generate direct thrust and do not involve the intermediate electrical power conversion stage.

In the context of strategic mission planning, this gives NEP a distinct advantage over NTP by potentially addressing multiple mission needs simultaneously. These potential advantages of NEP are multifaceted: it could mitigate the operational challenges of power generation in the unpredictable Martian environment, reduce payload mass requirements, and accelerate the maturation of critical nuclear technologies essential for sustained deep-space exploration.

Appendix B

Trajectory Modeling Python Code

The following code was developed in Python using the poliastro library to develop 3-D plots (seen in figures 3.4, 3.7, 3.8, and 3.9) of outbound transfer orbits (solved for using poliastro's Lambert problem solver) between Earth and Mars for input launch and arrival dates.

Listing B.1: Python code for Poliastro-based mission trajectory analysis

```
1  
2 import numpy as np  
3 import pandas as pd  
4 from astropy import units as u  
5 from astropy.time import Time  
6 from poliastro.bodies import Earth, Mars, Sun  
7 from poliastro.ephem import Ephem  
8 from poliastro.maneuver import Maneuver  
9 from poliastro.util import time_range  
10 from poliastro.twobody import Orbit  
11 from poliastro.plotting import OrbitPlotter3D  
12  
13 from astropy.coordinates import solar_system_ephemeris  
14  
15 solar_system_ephemeris.set("jpl")  
16
```

```

17 #ignore leap-second warning
18 import warnings
19 from astropy.utils.exceptions import ErfaWarning
20
21 warnings.simplefilter('ignore', ErfaWarning)
22
23
24 # Initial data
25 date_launch = Time("2038-06-01_15:02", scale="utc").tdb
26 date_arrival = Time("2039-01-07_05:17", scale="utc").tdb
27
28 print(date_arrival)
29
30 earth = Ephem.from_body(Earth, time_range(date_launch, end=date_arrival))
31 mars = Ephem.from_body(Mars, time_range(date_launch, end=date_arrival))
32
33 # Solve for departure and target orbits
34 orb_earth = Orbit.from_ephem(Sun, earth, date_launch)
35 orb_mars = Orbit.from_ephem(Sun, mars, date_arrival)
36
37 # Solve for the transfer maneuver
38 man_lambert = Maneuver.lambert(orb_earth, orb_mars)
39 dv_a, dv_b = man_lambert.impulses
40
41 # Get the transfer and final orbits
42 orb_trans, orb_target = orb_earth.apply_maneuver(man_lambert, intermediate=
    True)
43
44 # Compute the magnitudes of the delta-v vectors
45 dv_departure_mag = np.linalg.norm(dv_a[1].to(u.km / u.s).value) # Convert m/s
    to km/s
46 dv_arrival_mag = np.linalg.norm(dv_b[1].to(u.km / u.s).value)
47

```

```
48
49 plotter = OrbitPlotter3D()
50 plotter.set_attractor(Sun)
51
52 # Plot Earth and Mars ephemeris positions
53 plotter.plot_ephem(earth, date_launch, label=f"Earth_at_launch_position_({
54     date_launch.iso})")
55
56 # Plot the transfer orbit
57 plotter.plot_trajectory(
58     orb_trans.sample(max_anomaly=180 * u.deg),
59     color="black",
60     label="Transfer_orbit",
61 )
```

Bibliography

- [1] N. J. P. Laboratory, “Mars 2020 perseverance rover raw images.” <https://mars.nasa.gov/mars2020/multimedia/raw-images/>, 2025. Accessed: 2025-04-25.
- [2] NASA Glenn Research Center, “Nuclear thermal propulsion systems,” 2025. Accessed: 2025-04-09.
- [3] R. Dyson, D. V. Rao, M. Duchek, C. Harnack, R. Scheidegger, L. Mason, A. Juhasz, L. Rodriguez, R. Leibach, S. Geng, and D. Goodell, “Nuclear electric propulsion brayton power conversion working fluid considerations,” in *Proceedings of the Nuclear and Emerging Technologies for Space (NETS-2022)*, (Cleveland, OH, USA), American Nuclear Society, NASA Glenn Research Center, May 8–12 2022. NASA Technical Report E-20018, Document ID: 20220002293.
- [4] NASA, “Human exploration of mars design reference architecture 5.0,” Tech. Rep. NASA-SP-2009-566-ADD, National Aeronautics and Space Administration (NASA), July 2009. p. 48.
- [5] R. Sanders, “Scientists find oceans of water on mars — it’s just too deep to tap,” 2024. Accessed: 2025-04-28.
- [6] NASA Glenn Research Center, “Specific impulse,” 2023. Accessed: 2025-04-17.
- [7] S. D. Howe, P. McClure, and S. K. Borowski, “A review of nuclear thermal propulsion development and future prospects,” *Acta Astronautica*, vol. 181, pp. 141–155, 2021.

- [8] J. Howell, L. Johnson, J. Hopkins, M. Raftery, S. Oleson, and D. Landau, “Assessment of low-thrust nuclear electric propulsion options for human mars missions,” Tech. Rep. NASA/TP-2016-219045, NASA, 2016.
- [9] G. P. Sutton and O. Biblarz, *Rocket Propulsion Elements*. John Wiley & Sons, 9 ed., 2016.
- [10] NASA, “Planetary fact sheet - metric.” <https://nssdc.gsfc.nasa.gov/planetary/factsheet/>, 2023. Accessed: 2025-04-19.
- [11] NASA Glenn Research Center, “Ideal rocket equation,” 2023. Accessed: 2025-04-16.
- [12] B. Palaszewski, “Mars research: Propulsion, life support, and in-situ resource utilization,” Tech. Rep. NASA/TP–20210026187, NASA Glenn Research Center, 2021. Accessed: 2025-04-16.
- [13] B. Palaszewski, “Mars landing vehicles: Descent and ascent propulsion design issues,” in *Mars Research*, p. Chapter 12, IntechOpen, 2022. NASA Technical Reports Server (NTRS) Document ID: 20210026187.
- [14] Obama Administration, “Human deep space exploration,” 2016. Archived content from the Obama Administration.
- [15] NASA, “Space launch system (sls),” 2024. Accessed April 2025.
- [16] D. Szirocki and H. Smith, “A review of design issues specific to hypersonic flight vehicles,” *Progress in Aerospace Sciences*, vol. 84, pp. 1–28, 2016.
- [17] National Academies of Sciences, Engineering, and Medicine, “Space nuclear propulsion for human mars exploration,” tech. rep., The National Academies Press, Washington, DC, 2021.
- [18] U.S. Air Force Materiel Command, “History in two: Manned nuclear aircraft program.” <https://www.afmc.af.mil/News/Article-Display/Article/2664365/>

history-in-two-manned-nuclear-aircraft-program/, 2021. Accessed: 2025-04-11.

- [19] NASA, “Nasa, darpa will test nuclear engine for future mars missions.” <https://www.nasa.gov/news-release/nasa-darpa-will-test-nuclear-engine-for-future-mars-missions/>, 2023. Accessed: 2025-04-11.
- [20] NASA Glenn Research Center, “Rockets systems area,” n.d. Accessed: 2025-04-12.
- [21] NASA, “Sputnik and the dawn of the space age,” 2007. Accessed: 2025-04-12.
- [22] Encyclopædia Britannica, “Anti-nuclear movement,” n.d. Accessed: 2025-04-12.
- [23] “Research, development, test evaluation, defense-wide, fiscal year 2024 budget estimates: Darpa volume 1,” tech. rep., U.S. Department of Defense, Office of the Comptroller, 2023. Accessed: 2025-04-11.
- [24] D. Buden, J. A. Angelo, and D. W. Culver, “Nuclear thermal propulsion stage systems analysis,” Technical Memorandum NASA-TM-105261, NASA Lewis Research Center, 1991. Available at: <https://ntrs.nasa.gov/api/citations/19910017902/downloads/19910017902.pdf>.
- [25] M. Gates, “An overview of the jupiter icy moons orbiter (jimo) mission, environments, and materials challenges,” Tech. Rep. NASA/TM-2012-216895, NASA, 2012. NASA Technical Report 20120016895.
- [26] E. Y. Choueiri, “A critical history of electric propulsion: The first 50 years (1906-1956),” *Journal of Propulsion and Power*, vol. 20, no. 2, pp. 193–203, 2004.
- [27] NASA, “A powerhouse in deep space: Gateway’s power and propulsion element,” 2023. Accessed: 2025-04-19.

- [28] S. K. Borowski, “Nuclear thermal rocket/vehicle design options for future nasa missions to the moon and mars,” Tech. Rep. NASA-TM-107026, NASA Lewis Research Center, 1995. NASA Technical Memorandum.
- [29] NASA, “Solar electric propulsion makes nasa’s psyche spacecraft go,” 2022. Accessed: 2025-04-28.
- [30] M. L. Belair, C. J. Sarmiento, and T. M. Lavelle, “Nuclear thermal rocket simulation in npss,” tech. rep., NASA Glenn Research Center, 2013.
- [31] Y. Li, Y. Zhou, X. Zhang, Y. Yang, and J. Ren, “Optimization of hybrid renewable energy systems for hydrogen production: A techno-economic-environmental perspective,” *Energy Reports*, vol. 8, pp. 11635–11650, 2022.
- [32] B. Mattfeld, C. Stromgren, H. R. Shyface, D. R. Komar, W. M. Cirillo, and K. E. Goodliff, “Trades between opposition and conjunction class trajectories for early human missions to mars,” *Space*, 2014.
- [33] J. L. Cano and the poliastro development team, “poliastro: Python library for astrodynamics — documentation.” <https://docs.poliastro.space/en/stable/>, 2024. Accessed: 2025-04-05.
- [34] Wikipedia contributors, “Lambert’s problem — wikipedia, the free encyclopedia.” https://en.wikipedia.org/wiki/Lambert%27s_problem, 2024. Accessed: 2025-04-05.
- [35] J. L. Cano and the poliastro development team, “Multirevolutions solution in lambert’s problem — poliastro documentation.” <https://docs.poliastro.space/en/stable/examples/Multirevolutions%20solution%20in%20Lamberts%20problem.html>, 2024. Accessed: 2025-04-05.

- [36] S. K. Borowski, “Nuclear thermal propulsion (ntp): Key to affordable human exploration of the solar system and beyond,” Technical Memorandum NASA/TM-2011-216362, NASA, 2011.
- [37] NASA, “Moon to mars architecture concept review white papers: Mars surface power generation challenges and considerations,” 2023. NASA Technical Report.